CZECH TECHNICAL UNIVERSITY IN PRAGUE
FACULTY OF ELECTRICAL ENGINEERING

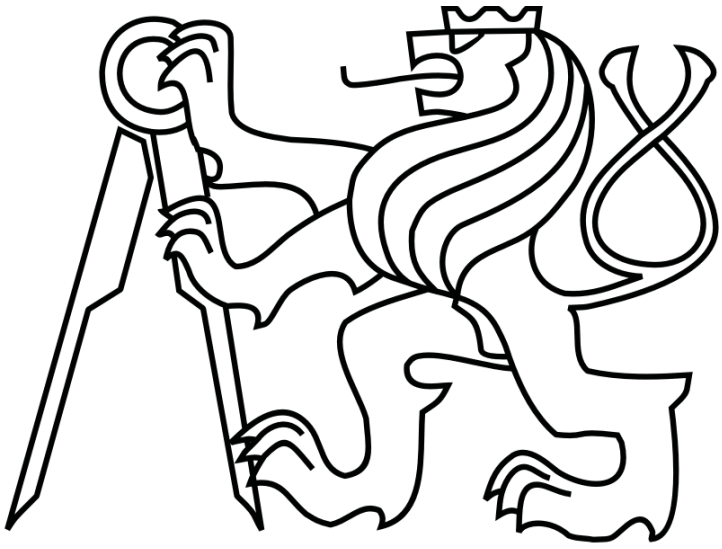

BACHELOR THESIS

VIBRATION SUPPRESSION IN INERTIAL SENSORS SIGNALS

Prague, 2011

Vladimír Kubelka

CZECH TECHNICAL UNIVERSITY IN PRAGUE
FACULTY OF ELECTRICAL ENGINEERING
DEPARTMENT OF MEASUREMENT

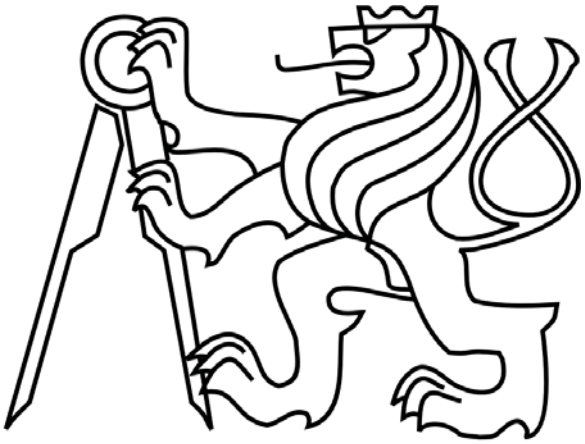

VIBRATION SUPPRESSION IN INERTIAL SENSORS SIGNALS

Bachelor Thesis Supervisor: *Ing. Michal Reinštein Ph.D.*

Prague, 2011 Vladimír Kubelka

ČESKÉ VYSOKÉ UČENÍ TECHNICKÉ V PRAZE
Fakulta elektrotechnická
Katedra měření

Akademický rok **2010-2011**

ZADÁNÍ BAKALÁŘSKÉ PRÁCE

Student:	**Vladimír Kubelka**
Obor:	**Kybernetika a měření**
Název tématu česky:	**Filtrace vibrací v signálech inerciálních senzorů**
Název tématu anglicky:	**Vibration Suppression in Inertial Sensors Signals**

Pokyny pro vypracování:

Cílem práce je implementace a porovnání kvality filtrů aplikovaných na signály inerciálních senzorů za účelem potlačení vibrací a zpřesnění odhadu navigačních veličin. Signály jsou měřeny inerciální měřicí jednotkou ADIS16405, která obsahuje tříosý akcelerometr a tříosý senzor úhlových rychlostí (rovněž i tříosý magnetometr). Jednotka bude umístěna na RC modelu letadla Bellanca Super DecathlonXXL za účelem sběru reálných dat. Součástí práce je analýza šumových vlastností inerciálních senzorů pomocí metody Allan variance.

Seznam odborné literatury:

[1] Hlaváč, V., Sedláček, M.: Zpracování signálů a obrazů. Skripta ČVUT Praha, 1.vyd. 2000
[2] Madisetti, V. K., Williams, D. B.: Digital Signal Processing Handbook. Atlanta, USA, 1999
[3] Meruane Naranjo, C.: Analysis and Modeling of MEMS based Inertial Sensors. Stockholm, 2008

Vedoucí bakalářské práce:	Ing. Michal Reinštein
Datum zadání bakalářské práce:	22. listopadu 2010
Platnost zadání do[1]:	3. února 2012

L.S.

Prof. Ing. Pavel Ripka, CSc.
vedoucí katedry

Prof. Ing. Boris Šimák, CSc.
děkan

V Praze dne 22. 11. 2010

[1] Platnost zadání je omezena na dobu dvou následujících semestrů.

DECLARATION

I declare that I have worked out this thesis independently and mentioned all used information sources in accordance with the *Guideline about observation of ethical principles while preparing college final thesis*.

In Prague, 23. 5. 2011

Vladimír Kubelka

ACKNOWLEDGMENTS

I would like to thank to my bachelor thesis supervisor Ing. Michal Reinštein, Ph.D. for advices and support during the work, to Ing. Martin Šipoš for help with accelerometers calibration and finally to my family for support during my undergraduate studies.

ABSTRACT

The goal of this work is to design, implement and compare digital filters in order to suppress vibrations in inertial sensors signals caused primarily by aircraft engines and therefore improve accuracy of inertial navigation. Inertial navigation is a way to determine position, attitude and velocity in space and is used in many civil, scientific and military applications, when other ways of navigation are not available or desired. Because the only leads for the inertial navigation are changes in acceleration or attitude of the navigated object, the quality of inertial sensors signals are vital.

The source of inertial data was a new micro-mechanical (MEMS) inertial sensor ADIS16405 (manufactured by Analog Devices) equipped with triaxial accelerometer, triaxial gyroscope and triaxial magnetometer. Quality of designed filters was tested using inertial signals affected by an experimental source of vibrations - an electric motor with deviated balance wheel - and by an RC model Bellanca Super DecathlonXXL. This work has also studied noise characteristics of the ADIS16405 sensor using the *Allan variance method*. These characteristics can be used for creating a mathematical noise model of the sensor necessary for estimation of random sensor errors.

KEY WORDS

Accelerometer, Allan Variance, digital filter, gyroscope, inertial navigation, MEMS, vibrations.

ABSTRAKT

Cílem práce byl návrh, implementace a zhodnocení číslicových filtrů za účelem potlačení vibrací v inerciálních signálech, způsobených především činností leteckých motorů, a s tím i vylepšení přesnosti inerciální navigace. Inerciální navigace je způsob, jak určit polohu, orientaci a rychlost v prostoru a je využívána v mnoha civilních, vědeckých i vojenských aplikacích, všude, kde nejsou k dispozici nebo žádoucí jiné způsoby navigace. Protože vyjma výchozího bodu jsou vstupními veličinami pouze změny rychlosti a orientace navigovaného objektu, je kvalita inerciálních signálů zásadní.

Zdrojem dat byl nový mikro-mechanický (dále MEMS) sensor ADIS16405 vyráběný firmou Analog Devices vybavený trojosým akcelerometrem, trojosým gyroskopem a trojosým magnetometrem. Kvalita navržených filtrů byla ověřena na experimentálních datech zatížených vibracemi. Vibrace byly generovány zprvu pouze jednoduchým motorkem s excentrickým setrvačníkem a poté změřeny na RC modelu letounu Bellanca Super DecathlonXXL. Tato práce se také zabývala parametry šumu výše zmíněného sensoru, a to za použití metody *Allan Variance*. Tyto parametry mohou být dále použity k vytvoření matematického modelu sensoru jako zdroje šumu, což je základní předpoklad k použití Kalmanovy filtrace – jednoho ze způsobů potlačení chyb navigace způsobených šumem a poruchami inerciálních signálů.

KLÍČOVÁ SLOVA

Akcelerometr, Allan Variance, číslicový filtr, gyroskop, inerciální navigace, MEMS, vibrace.

CONTENTS

1 INTRODUCTION

The aim of this work was to analyze noise produced by the inertial sensor ADIS16405, a new product of Analog Devices, which offers inertial and magnetic measurements in one package for a considerable cost and to cope with vibrations, which could degrade accuracy of inertial navigation. Noise terms were analyzed by a time-domain-based method called Allan Variance (Allan, 1966), (El-Sheimy, Hou, & Niu, 2008), which is suitable for this problem. The problem of vibrations was modeled by an electric motor equipped with an eccentric balance wheel; filters were designed to suppress errors in attitude mechanization. Model data were verified by measuring vibrations of a RC aircraft Bellanca Super DecathlonXXL.

Today, there are many means of navigation – which is basically a way of determining position and attitude in space – and most of them rely on the information from an external source. The most natural, yet difficult to implement (Sazdovski, G., & Tsourdos, 2010), is navigation based on observing surroundings and comparing it with a map. Other means of navigation, which are used today in aerospace applications, are based on information transmitted using radio waves (for *example VHF Omnidirectional Radio Range*). A commonly used technology is GPS which uses satellites orbiting the Earth and transmitting exact value of their atom clocks. A receiver combines signals from several satellites and computes its exact time, position and altitude.

As said before, all these means of navigation rely on the external source of information. However, there are applications where this approach is not desired, not possible or not accurate enough. An example of a case, in which these are not desired, is a submarine, which would risk revealing its position by surfacing in order to receive a GPS signal. Another example is a spacecraft, which cannot use any of the mentioned means of navigation. Also, if a high accuracy is required, these means may not be adequate, the well-known problems are low refresh rate (GPS), possible jamming or signal outage.

For these applications, an inertial navigation may be used. It is based on measuring changes in velocity as well as angular velocities of the navigated object, integrating them and transforming into one of the defined navigation frames (Shin, 2005), (Savage, 1998a), (Savage, 1998b). Inertial navigation can provide accurate information (El-Sheimy, Hou, & Niu, 2008, p. 1), but quickly degrades with longer time periods (for example, bias in accelerometer signal will cause error comparable to $x(t^2)$). This phenomena is caused by the fact, that along with useful signal, inertial sensors produce noise and even the useful signal contains variety of errors caused by vibrations produced by a propulsion system of a vehicle, by roughness of a surface (in case of terrestrial vehicles) and others.

1.1 Low-Cost MEMS Sensors

Progress in micro-mechanical technologies allowed fabrication of whole inertial sensors integrated onto single silicon chip, diminishing the size and cost aspects. Micro-mechanical (MEMS) technology refers to devices of a typical length of less than 1 mm but more than 1 µm combining integrated circuits as well as mechanical (often vibrating or deforming) parts (Meruane, 2008). These devices use standard integrated circuit batch-processing fabrication technology, allowing them to be produced in current factory installations.

The obvious advantages are redeemed by lower performance – behavior of a thin-film materials significantly differ from their macroscopic counterparts. Especially homogeneity of the material and potential structural disorders may significantly affect the performance of a MEMS device (Meruane, 2008, p. 11).

1.2 ADIS16405

In order to collect inertial signal data, a new product of Analog Devices – ADIS16405 – was provided (Figure 1.1 and Figure 1.2). ADIS16405 is an inertial sensor combining triaxial accelerometer, triaxial gyroscope and triaxial magnetometer. It is factory calibrated for sensitivity, bias, alignment and linear acceleration (gyroscope bias). These are supposed to assure accurate inertial measurements over a temperature range of -40°C to 85°C (Analog Devices, 2009).

Figure 1.1 ADIS16405 with an evaluation board

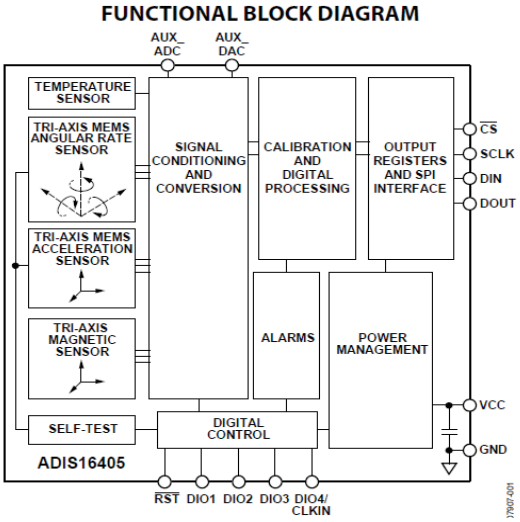

Figure 1.2 ADIS16405 block diagram (Analog Devices, 2009)

The sensor interface is SPI compatible; however, an original evaluation board was used to collect the data and to test its performance. Analog Devices provide an USB driver and simple software, which can display all sensor output values, set sensor registers and log selected signal into CSV compatible text file. The provided software was used for all ADIS measurements in this work.

2 THEORETICAL BACKGROUND

2.1 ACCELEROMETERS AND GYROSCOPES

It is often said that an **accelerometer** measures acceleration diminished by Earth gravitational field; however this concept is not correct. Attitude of the accelerometer has critical influence on the way gravity affects the output signal. According to (Savage, 2005a, p. 2), an accelerometer is an inertial sensor measuring projection of a specific force on its sensing axis. Specific force is defined as "*the time rate of change of velocity relative to local gravitational space. Local gravitational space is then defined as the same space occupied by the accelerometer but which contains a virtual mass with zero applied specific force.*"

The basic principle of accelerometer operation is sensing a proof mass motion relative to sensor case or torque required to maintain the proof mass in a zero position relative to the case (Meruane, 2008, p. 12). Simple mechanical model is proposed in Figure 2.1:

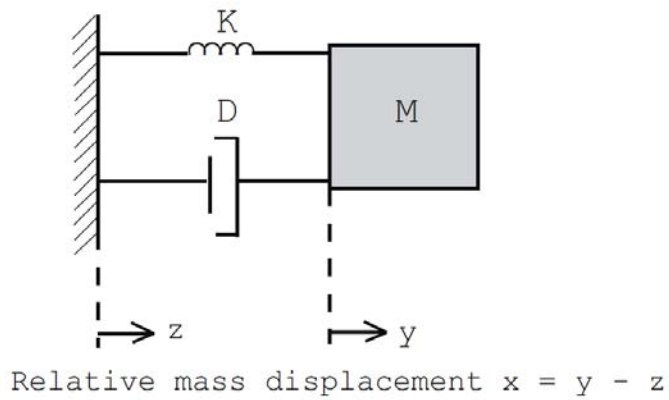

Figure 2.1 Mechanical model of an accelerometer (Meruane, 2008, p. 13)

Typical micro-mechanical implementation of this model is displayed in Figure 2.2. Displacement of the central proof mass attached to the silicon chip by suspension beams is measured by series of capacitors formed by the "comb" structure.

An inertial sensor measuring angular rate relative to inertial space is called angular rate sensor or more usually **gyroscope**. There are three basic principle of gyroscope operation: momentum of a spinning rotor, the Coriolis Effect on a vibrating mass and the Sagnac interference effect on an optical fiber-coil (Fiber Optic Gyroscope) (Curey, Ash, Thielma, & Barker, 2004) and on a ring laser (Ring Laser Gyroscope).

The classical approach is the utilization of a spinning rotor (*gyroscope*), whose angular momentum tends to keep the axis of rotation in one direction. This is a robust solution; however, the quality of the sensor signal is dependent on the angular momentum, which is proportional to the velocity of rotation and to the moment of inertia. Both these factors are difficult to be realized using MEMS

technology. To decrease the number of moving parts, Sagnac interference based gyroscopes are used in tactical grade applications. This technology is very accurate, yet expensive. The main principle is that a light beam propagates through an optic fiber at speed lover than *c*, while it can be accelerated by a movement of the fiber.

The last mentioned approach is the Coriolis Effect. It can be derived as a second derivative of position vector relative to non-inertial rotating system by time, resulting into fictional force causing side acceleration while moving forward. Similar effect occurs with vibrating mass; vibration in one direction (while angular velocity is nonzero) causes vibration in a perpendicular direction. Simple schematics are shown in Figure 2.3.

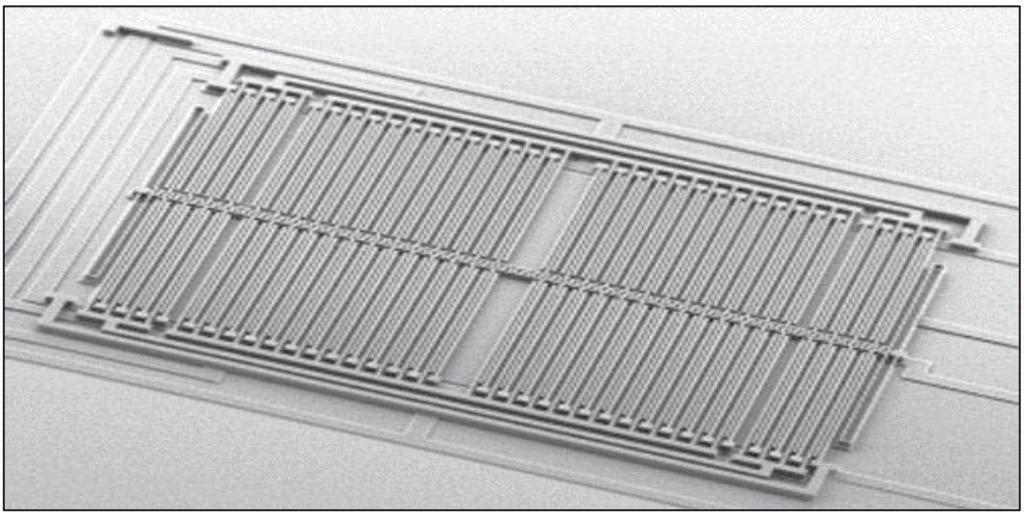

Figure 2.2 Typical MEMS implementation of an accelerometer; the *comb* structure (SensorDynamics, 2011)

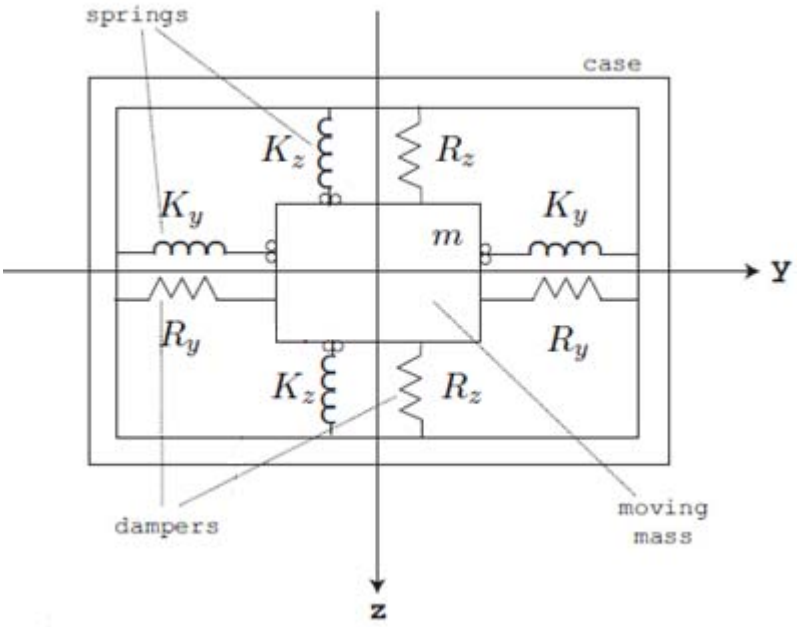

Figure 2.3 Schematics of the Coriolis Effect based gyroscope; *m* is a vibrating mass (Meruane, 2008, p. 15)

2.2 Noise and Deterministic Errors in Inertial Signals

There is no sensor that could measure with absolute accuracy. Unfortunately, the process of the inertial navigation is very sensitive to errors of the measured inertial quantities. The indicated position and attitude will degrade with time cubed and time respectively if a bias is present in the signal.

Imperfections are especially observed in low-grade inertial sensors and ADIS 16405 belongs to this category; therefore noise analysis is critical for the quality of navigation. The general composition of an inertial sensor signal is shown in Figure 2.4.

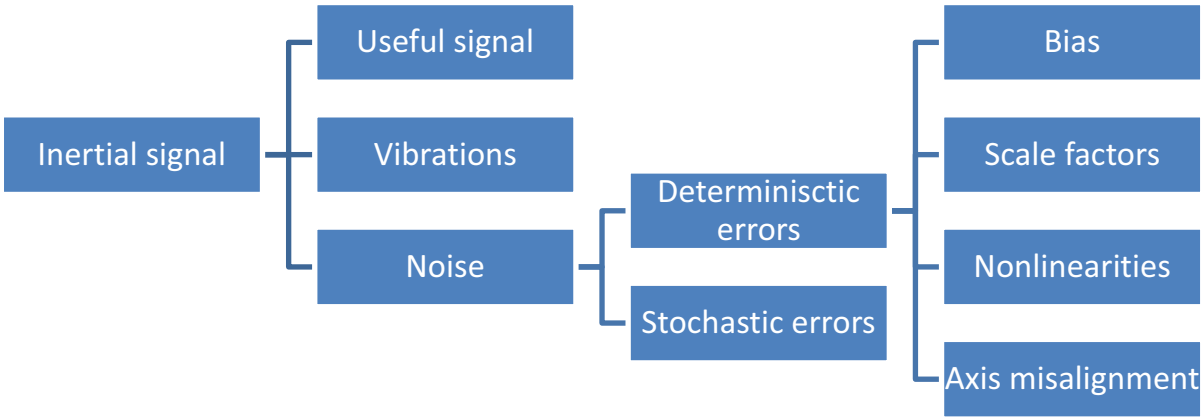

Figure 2.4 Composition of an inertial sensor signal

Useful signal is the only part of the signal that contains useful information for the inertial navigation corresponding to the motion dynamics of the navigated object. It is composed of specific force measured by accelerometers and angular velocity measured by gyroscopes, while these ones are actually performed by the navigated vehicle/object.

Vibrations are dynamics of a vehicle measured by the inertial sensors, which are not useful for the process of navigation. They may be caused by a propulsion system of the vehicle, by roughness of the surface (in a case of a surface vehicle), by air turbulences etc. In theory, perfectly working inertial navigation should cancel the influence of vibrations in the same way the navigated vehicle does (i.e. minimally changing the vehicle trajectory), however quantization, limited sampling frequency and other nonlinearities in the navigation process chain cause the fact that vibrations degrade navigation accuracy. The impact of vibrations can be diminished by setting correctly the physical connection between the IMU and the vehicle (vibration damping) or by the signal preprocessing. Several filters have been proposed in this work to resolve this issue.

Noise is a part of the inertial signal, which does not have the origin in the dynamics of the navigated vehicle. Noise is produced by the inertial sensor itself and can be characterized into two main parts: the stochastic and the deterministic errors.

Stochastic errors are caused by physical processes on the microscopic level and cannot be analytically expressed as a function of a time; therefore, they are concerned to be random. Effect of stochastic errors is called bias drift (Meruane, 2008, p. 16) and can be modeled as response of a theoretical system to white noise (Allan, 1966). One of the way to cope with stochastic errors is the Kalman filter, which utilizes mathematical model of the navigated system including all errors, and estimates the navigation errors, which can be used to correct the navigation trajectory (Reinštein, 2011), (Shin, 2005).

Deterministic errors are caused by sensor fabrication imperfections and can be determined by calibration (Šipoš, 2010). As soon as determined, effects of deterministic errors can simply be reverted. Several subcategories are distinguished:

Bias is a constant value added to the signal, which doesn't vary with time; however, it can be a function of temperature. In that case, the dependence can by approximated by a polynomial function (Meruane, 2008, p. 26).

Scale factor expresses the difference between the nominal and true sensitivity of the sensor. It can be related to temperature in the same way as bias can; in that case, the same approach is chosen.

Nonlinearities are deviations from ideally linear relation between input quantity and output signal. This one and two previous are shown in Figure 2.5.

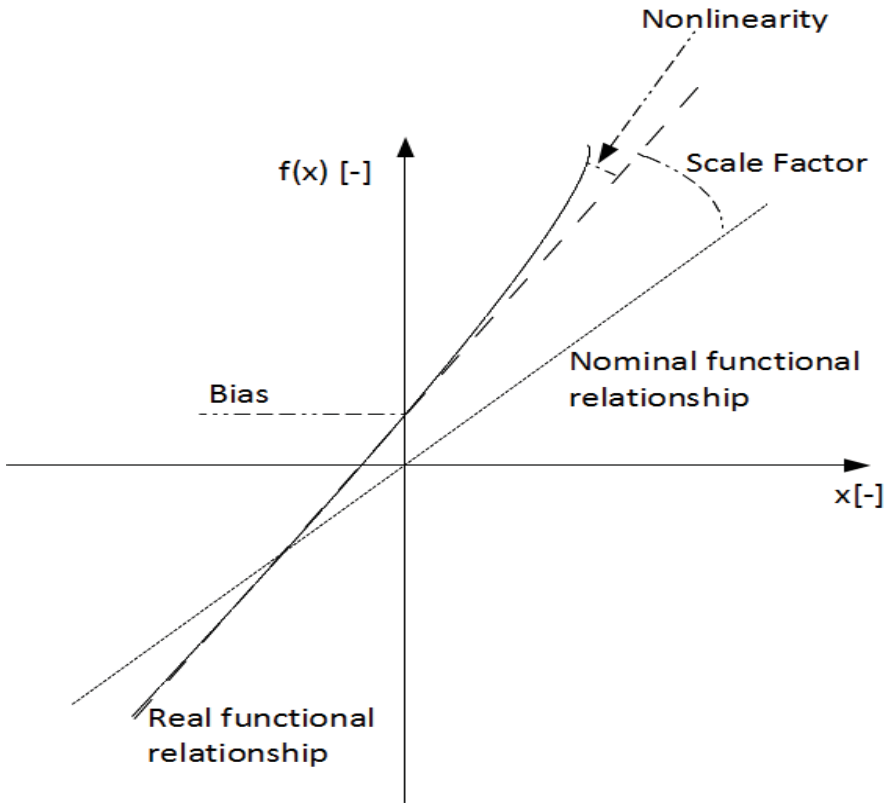

Figure 2.5 Some of deterministic errors; the line with *slope = 1* is a nominal functional relationship between measured quantity and the sensor output signal; the other solid curve expresses a real functional relationship of the sensor

Axis misalignment is caused during fabrication process by misaligning sensor elements; in the case of ADIS16405, there are triaxial sensors, therefore three sensor elements per sensor to be aligned orthogonally in such a way that their sensing axes are orthogonal. If this condition is not fulfilled, the measured vector projected to the sensing axes is subsequently incorrectly interpreted, because orthogonal measurement system is expected. This may be one of the causes of signal nonlinearities mentioned above. However, this error can be corrected by applying transformation matrix from the sensor system to the orthogonal one. The problem is outlined in Figure 2.6.

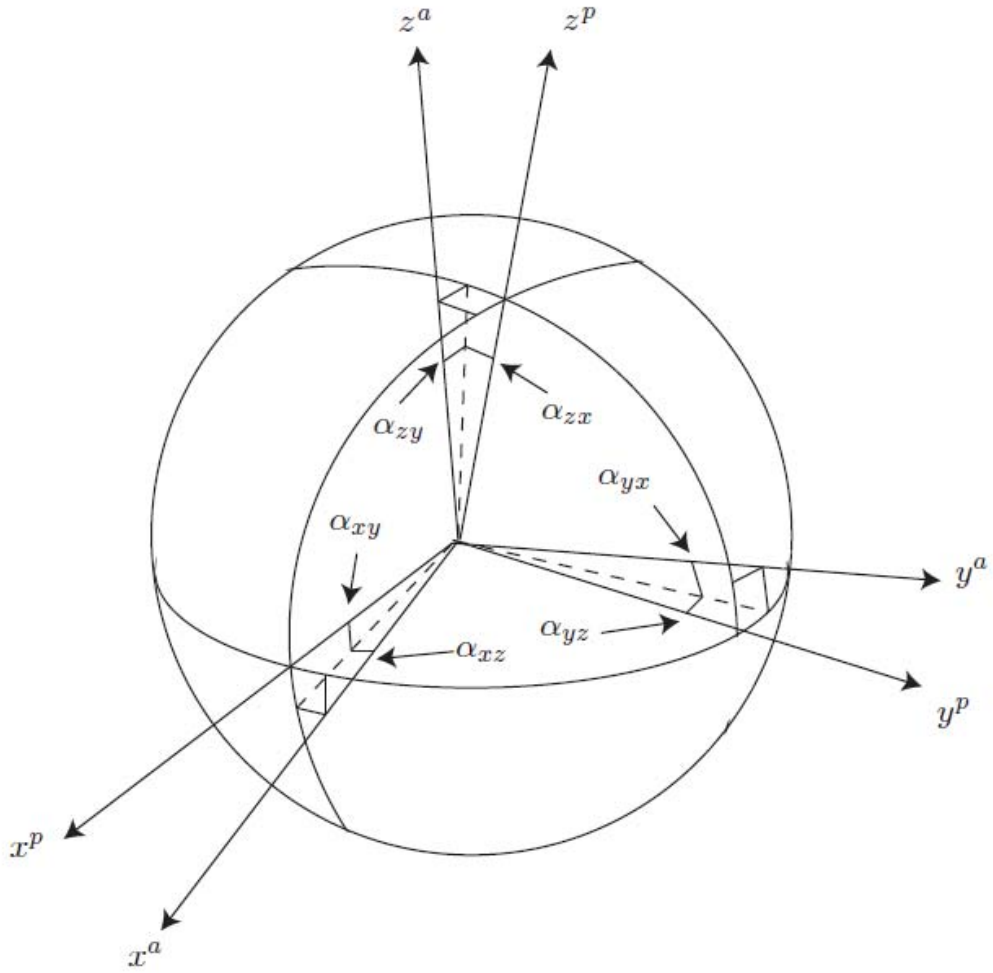

Figure 2.6 Axis (x^a, y^a, z^a) misalignment with platform orthogonal system (x^p, y^p, z^p) expressed by misalignment angles α (Skog & Händel, 2006)

2.3 ALLAN VARIANCE

Stochastic noise present in the signal can be analyzed by evaluating its *power spectral density* (PSD), which shows distribution of noise power as a function of frequency. It can be evaluated from its correlation function using Wiener–Khinchin theorem (Sedláček, 2009):

$$S_{XX}(e^{j\theta}) = \sum_{r=-\infty}^{\infty} R_{XX}(x)e^{-jr\theta} \tag{2.1}$$

where ***S*** is the PSD, $\boldsymbol{R_{XX}}$ is autocorrelation function and $\boldsymbol{\vartheta}$ is normalized frequency. Another approach is the Welch method (Welch, 1967, pp. 70-73) based "*on Time Averaging Over Short, Modified Periodograms".* Both of these methods lead to frequency domain analysis (El-Sheimy, Hou, & Niu, 2008).

In this work, time-domain analysis method called **Allan Variance** (AVAR) was chosen. This method was firstly proposed by D.W. Allan in 1966. It was originally developed to study noise in precise Cesium oscillators (Allan, 1966). However, it is suitable for any precision measurement instrument. The advantage of AVAR method is that when plotted in logarithmic scales on both axes one can easily differentiate various noise terms present in the analyzed signal (Meruane, 2008).

The AVAR is representation of RMS random-drift errors as a function of averaging times (El-Sheimy, Hou, & Niu, 2008). To evaluate it, measured data are divided into groups called clusters of length from *1* to *N/2* where *N* is number of all measured samples. See Figure 2.7.

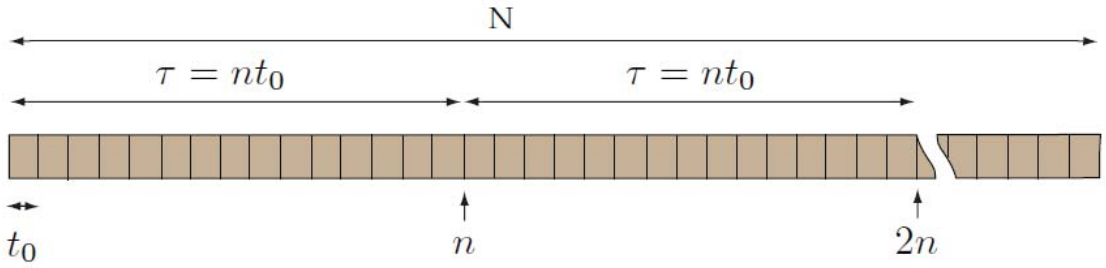

Figure 2.7 Scheme of data structure use in AVAR; the whole data set is divided into clusters of length *n* (Meruane, 2008, p. 32)

Each cluster is associated with $\tau = nt_0$ where t_0 is sampling period. There are $K = N/n$ clusters, an average of each one is computed (Lawrence, 1993):

$$\overline{\omega}_k = \frac{1}{n}\sum_{i=1}^{n} \omega_{(k-1)n+i} \tag{2.2}$$

where ω_k is k^{th} measured sample.

Subsequently, AVAR is defined for averaging time $\tau = n/f_s$ as:

$$\sigma^2(\tau) = \frac{1}{2(K-1)} \sum_{k=1}^{n-1} (\overline{\omega_{k+1}}(M) - \overline{\omega_k}(M)) \tag{2.3}$$

Different averaging times τ can be chosen as long as the condition of cluster length smaller than $N/2$ is not violated. If plotted in logarithmical plot, various noise sources simply by examining the graph slope.

The relationship between AVAR and two-sided power spectral density can be written as:

$$\sigma^2(\tau) = 4 \int_0^{\infty} S(f) \frac{\sin^4(\pi f \tau)}{(\pi f \tau)^2} df \tag{2.4}$$

where the specific term $sin^4(x)/x^2$ is a result of the method of creation and operation on the clusters (El-Sheimy, Hou, & Niu, 2008, p. 142). This equation is used to identify noise terms and their parameters analyzing the AVAR plot. Generally, several noise terms can be found in one signal, next paragraphs will discuss their origin. Their mathematical expressions in terms of PSD and AVAR are summarized in Table 2.1, mathematical derivation can be found at (El-Sheimy, Hou, & Niu, 2008, pp. 142-144). All mentioned noise terms are shown in Figure 2.8.

Quantization Noise is caused by quantization during digitalization of the analog signal. This noise term can be identified as a slope of -1 in the log-log plot. Magnitude of the quantization noise can be found at $\tau = 3^{1/2}$ s.

Angle (Velocity) Random Walk is a noise term causing small varying drift of angle/velocity by integrating wide-spectrum noise. This term can be considered the main source of errors in inertial sensors (Reinštein, 2011, p. 22). In a log-log plot, it can be identified as a slope of -1/2 and its coefficient expressed in a unit [m/s/h$^{1/2}$] or [°/h$^{1/2}$] can be read at $\tau = 1$ s.

Bias Instability also known as "*1/f noise*" or "*flicker noise*" is a low frequency fluctuation caused by electronics and other components susceptible to flickering (Keshner, 1982). Allan standard deviation of this term starts with a slope of +1 and after reaches its cutoff frequency asymptotically. Limit of bias instability ([m/s/h] or [°/h]) can be read at the flat region.

Rate Random Walk is a noise term of an uncertain origin. It can be identified by slope of 1/2 and magnitude of this noise is to be read off at $\tau = 3$ s (IEEE, 1998).

Rate Ramp is rather deterministic than random process. Its influence can be compared to very slow acceleration during several hours. The magnitude can be read slope of +1 at time $\tau = 2^{1/2}$ s.

Exponentially Correlated Noise and **Sinusoidal Noise** are not significant for inertial sensor signals and were not considered in this work.

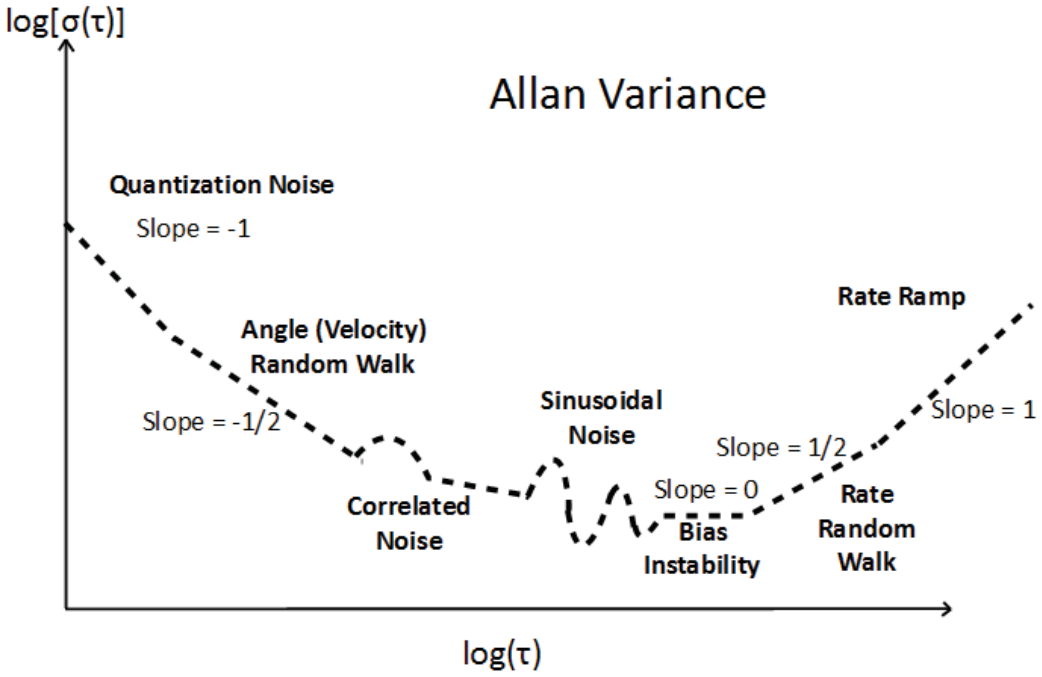

Figure 2.8 Sample AVAR plot according to (Meruane, 2008, p. 43)

Noise Type	Units	Slope	Root Allan Variance	Parameter of interest
Quantization noise	[m/s] or [°/s]	-1	$\sigma = \frac{\sqrt{3}Q}{\tau}$	Q
Angle (Velocity) Random Walk	[m/s/h$^{1/2}$] or [°/h$^{1/2}$]	-1/2	$\sigma = \frac{N}{\sqrt{\tau}}$	N
Bias Instability	[m/s/h] or [°/h]	0	$\sigma = 0.664B$	B
Rate Random Walk	[m/s/h/h$^{1/2}$] or [°/h/h$^{1/2}$]	+1/2	$\sigma = K\sqrt{\frac{\tau}{3}}$	K
Rate Ramp	[m/s/h^2] or [°/h^2]	+1	$\sigma = \frac{R\tau}{\sqrt{2}}$	R

Table 2.1 Summary of noise terms in AVAR method (Reinštein, 2011, p. 24)

2.4 SIGNAL PROCESSING

2.4.1 FIR AND IIR FILTERS

Finite Impulse Response (FIR) and Infinite Response Filters (IIR) are digital filters are intended for alteration of digital signal spectra. They are composed of three basic components: summer, amplifier and unit delay (Figure 2.9).

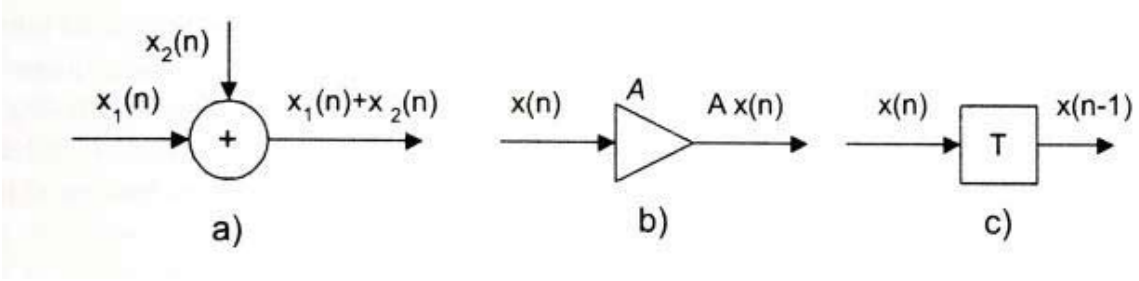

Figure 2.9 Basic digital filter components: a) summer b) amplifier c) unit delay (Sedláček, 2009, str. 57)

FIR filters according to their notation always have finite impulse response. FIR filters can be designed as a structure with or without feedback; however, the most common structure is the transversal one (Figure 2.10). FIR filters are always stable, yet to obtain comparable transfer function to a corresponding IIR filter, FIR filter is designed with much higher order (i.e. its structure contains more unit delays); hence, FIR filter brings longer delay to the signal (Sedláček, 2009).

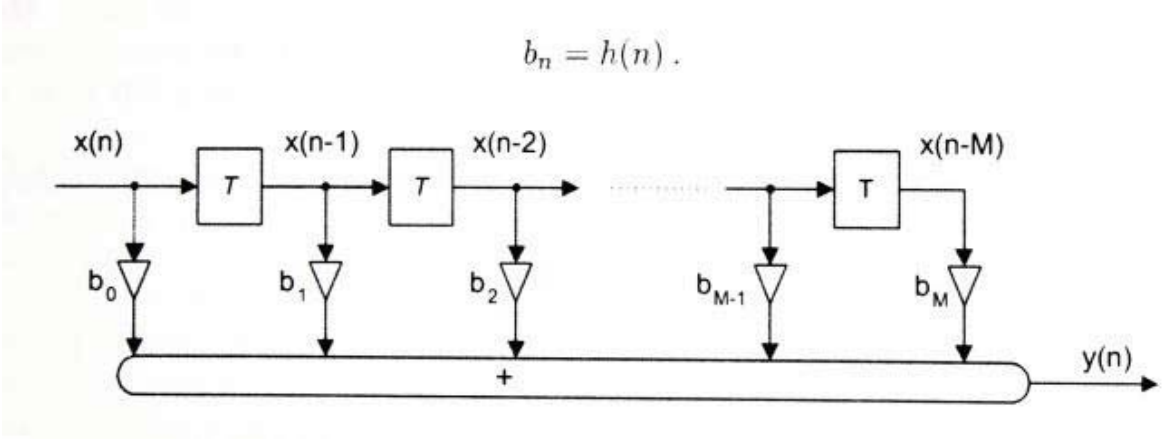

Figure 2.10 Transversal structure of a digital filter (Sedláček, 2009, p. 58)

IIR filters have infinite impulse response; therefore, the only possible structure is the one containing feedback (Figure 2.11). They are of a lower order bringing shorter delay to the signal but they can become unstable and oscillate (Sedláček, 2009).

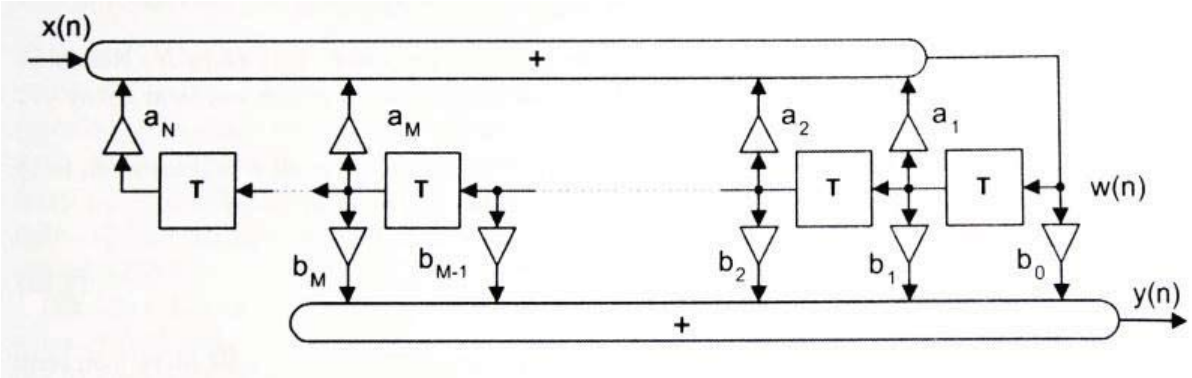

Figure 2.11 The second direct structure of a IIR filter (Sedláček, 2009, p. 62)

To design a filter, two approaches can be chosen from. It is possible to design an analog counterpart and then transfer it to the digital form. The second approach is straightforward design of a filter, often using a computer tool. Mathematical background of digital filters is thoroughly discussed in Chapter 4 in (Sedláček, 2009) and is not an object of this work. To design desirable filters, a computer tool was used, namely ***fdatool***, which is a GUI of the *Signal Processing Toolbox* ^{TM} distributed as a part of *Mathworks MATLAB.* This one provides intuitive tool for designing FIR and IIR filters; method of design, nominal frequencies and type of filter are selected and based on these, fdatool generates necessary filter coefficients.

Moving Average is a special case of a FIR filter. It can be designed as a structure both with and without feedback. According to its name, MA filter provides average over last *N* digital samples, where *N* is the order of the filter. MA filter can suppress undesired sinusoidal signal, whose period length is equal to $N \cdot T_s$ where T_s is the signal sampling period. For this work, own *MATLAB* implementation of the MA filter was written:

```
function data_out = mov_aver(data_in, span)

    if(span <2)
        error('Span is permitted 2 and higher');
    end

    len = length(data_in);
    data_out = zeros(1, len);

    for n = 1:span
        data_out(n) = sum(data_in(1:n))/n;
    end

    inv span = 1/span;

    for n = (span+1):len
        data_out(n) = sum(data_in((n+1-span):n))*inv_span;
    end

end
```

2.4.2 *WAVELET TRANSFORMATION AND DE-NOISING*

Fourier transform provides a powerful tool for signal analysis, allowing decomposition of a signal into series of harmonic elements; yet, because Fourier operates upon a signal as a whole, local analysis is impossible. Hence, Fourier transform is not sensitive to short and isolated events in the signal ((MathWorks, 2008)-Help-section Wavelet analysis). This issue can be partially solved by application of Short Time Fourier Analysis; nevertheless this approach requires choice of a fixed-length window, which is used to portion signal into shorter clusters and transform each one using Fourier transform. However, there may be signals that require more flexible approach.

Wavelet analysis offers ability to perform a local analysis as well as a global one. Wavelet method is based on a process of windowing a signal with a *wavelet* window of various width and shift. The process of obtaining a continuous Wavelet transform of a signal can be expressed as (Strang & Nguyen, 1997):

$$CWT(a,b) = \frac{1}{\sqrt{a}} \int_{-\infty}^{\infty} x(t)\Psi(\frac{t-b}{a})\mathrm{dt} \tag{2.5}$$

where ***a*** and ***b*** are scaling and shifting factor. The function Ψ is a wavelet window, which is not strictly defined. The conditions are that it must be oscillatory, zero average, short and converging rapidly to zero on both ends (Abdel-Hamid, 2005). By shifting the wavelet, distinguished time periods can be examined. Reciprocally, by scaling the wavelet, distinguished frequency domains can be examined. The process of shifting and scaling is shown in Figure 2.12.

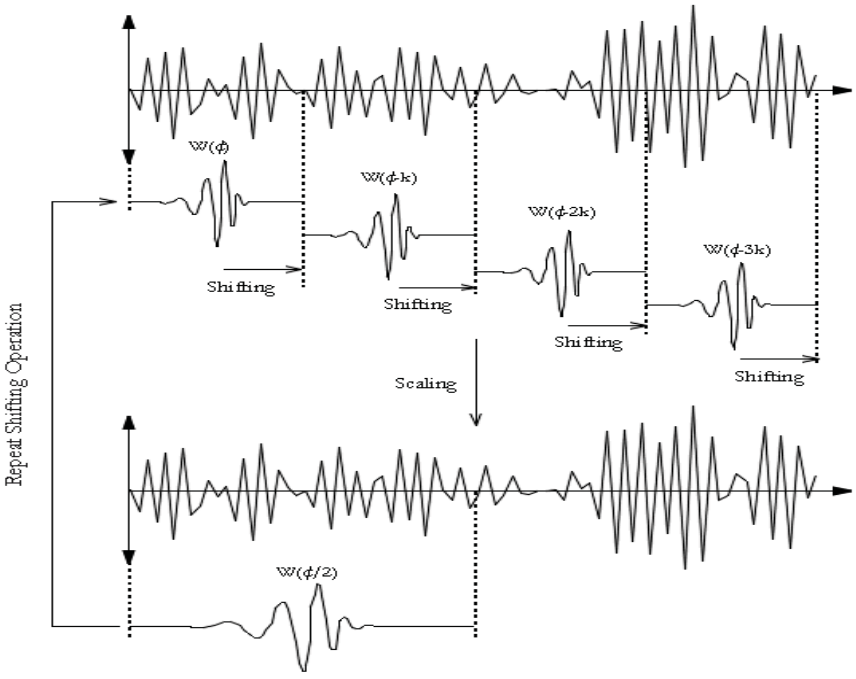

Figure 2.12 The process of shifting and stretching a wavelet window over a transformed signal (Altmann, 1996)

Enumerating (2.5), *wavelet coefficients* are obtained. Plotting them, a complete overview on the signal time as well as frequency qualities is obtained. A discrete counterpart of the continuous wavelet transform can be expressed using summation instead of integration, see the formula 4.3 at (Abdel-Hamid, 2005, p. 85).

Based on the discrete wavelet transform, multi-resolution analysis can be defined. Common inertial signal contains low-frequency components of our interest and also high-frequency ones, which are often connected with noise and vibrations. Wavelet multi-resolution analysis allows the signal to be decomposed into these low-frequency components (called *approximations*) and high-frequency components (called *details*) using corresponding high-pass and low-pass filters. Each set of these filters is adherent to a specific wavelet window (see *Relationship of Filters to Wavelet Shapes* in (MathWorks, 2008)). The process of decomposition can be repeated several times obtaining various levels of decomposition. Apart from the level of decomposition, the original signal can be reconstructed. However, we can select some approximations or details, which are not desirable to be part of the signal and replace them with zeros. This is basically the process of wavelet denoising, while the selection of unfitting approximations or details is called *Thresholding* and is discussed in (Reinštein, 2011, p. 29). An example of wavelet multi-resolution analysis is shown in Figure 2.13. In this work, **Wavelet toolbox** ™ denoising function **wden** was used.

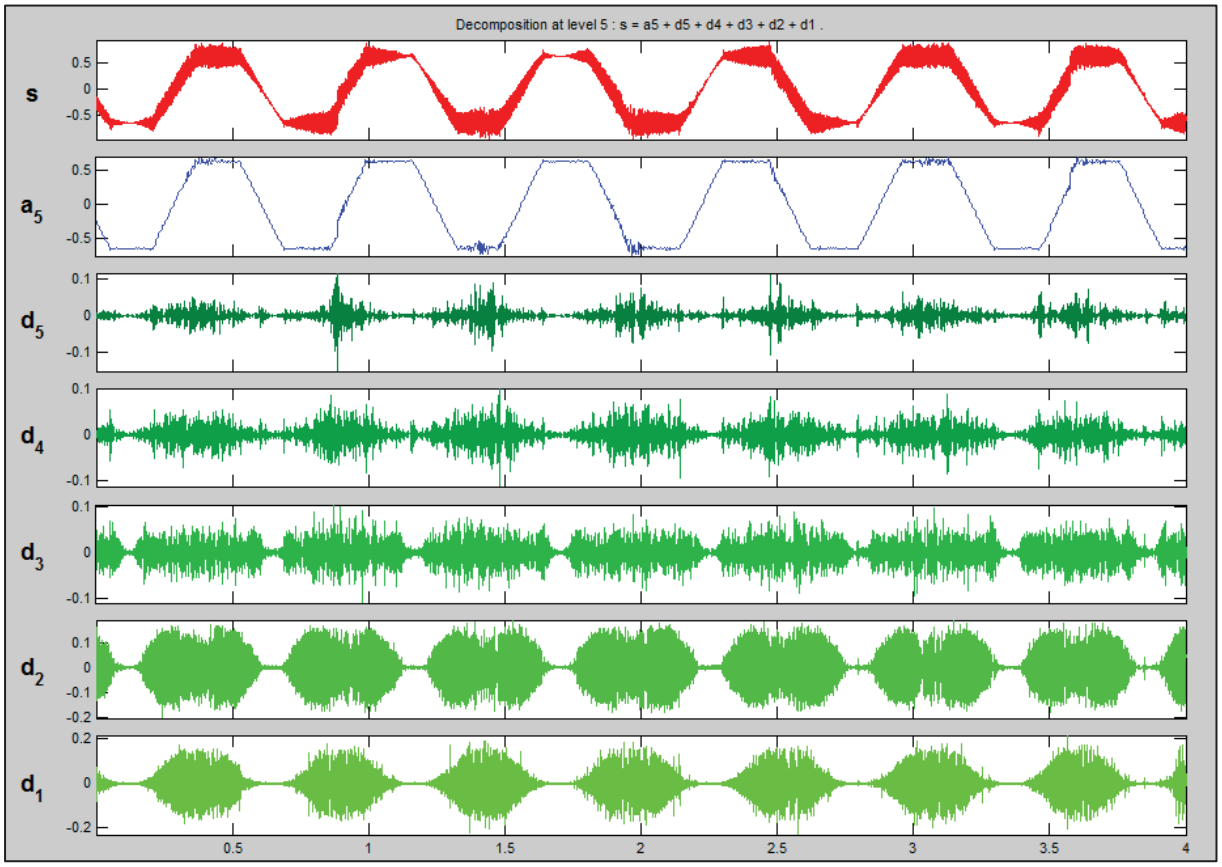

Figure 2.13 Example of a wavelet multi-resolution analysis (***s***: signal, $\boldsymbol{a_5}$: approximation at level 5, $\boldsymbol{d_x}$: details)

3 ATTITUDE MECHANIZATION

To correctly review quality of the proposed filters, several possibilities were taken into account. To evaluate the effect of the filters on the position mechanization, a double integration of the accelerometer data was considered. This approach brought several problems. Without any accurate reference while performing dynamical test, reliable conclusions were impossible to make. This would only leave a possibility of static measurement with the aim of stopping computed position information from drifting. This could lead to filters, which would degrade dynamical properties of the navigation.

To avoid these difficulties, different approach was chosen. An algorithm for mechanization of the navigation equations was proposed, which would compute only attitude vector disregarding position coordinates. Attitude vector can be compared to a reliable reference of a calibration table RoTiP (Annex B) which was available. The reconsideration of the position mechanization was left for future work. The algorithm in this configuration can be used for example for data fusion for an artificial horizon – the attitude meter, which does not need information about vehicle's position. As shown below, the algorithm uses both gyroscope and accelerometer data, hence the filters for both types of inertial sensors can be designed and evaluated. The algorithm is based on the mechanization algorithm (Reinštein, 2011, pp. 64-70) which contains a complete mechanization solution including Kalman filtering. Only parts necessary for attitude mechanization were selected so the filters could be evaluated. The mechanization algorithm does not need any other input than the inertial sensor signals and optional initial heading information. The algorithm was tested by post-processing; nevertheless, it can be used as a real-time application due to its low computational requirements. A complete mechanization algorithm realization in MATLAB environment which does not involve Kalman filtering can be found in (Burian, 2009).

The mechanization algorithm uses four attitude representations in various space frames; *Euler angles, Direction Cosine Matrix (DCM), Rotation vectors and Quaternions*. The algebra behind these representations is thoroughly discussed in (Savage, 1998a), (Savage, 1998b), (Shin, 2005, pp. 9-18), (Reinštein, 2011, pp. 31-34). To shortly sum basic their basic properties:

Euler angles were originally developed by Leonhard Euler as a representation of orientation in Euclidean space (Reinštein, 2011, p. 31). It is a natural way to describe attitude using terms *Roll*, *Pitch* and *Yaw angles.* Change in roll is understood to be a movement around vehicle axis leading from a nose of the vehicle to its tail. Similarly, change in pitch corresponds to movement around an axis perpendicular to the previous one, going through the center of gravity of the vehicle and parallel to the surface. Yaw angle represents azimuth in a common sense.

DCM matrix is a transformation matrix composed of three perpendicular rotations corresponding to the three Euler angles. For mathematical interpretation, see formula (4-38) in (Reinštein, 2011, p. 31).

Quaternion is a vector containing scalar and vector part. It is an equivalent to DCM; yet being used for its mathematical advantages. Various transformations to other attitude representations can

be found in the mentioned papers. For quaternions, inversion and multiplication is defined (different from standard vector multiplication), see formulas (2-2) and (2-3) in (Shin, 2005, p. 11).

Rotation vector is the last used representation. It is a three-dimensional vector that origins in the frame origin and whose direction coincides with the axis of the rotation. Its Euclidean norm determinates the magnitude of rotation (Reinštein, 2011).

The representations mentioned above always transform one spatial frame to another. There are several frames commonly used in navigation, this work uses *Earth-Centered Inertial Frame (I-frame)*, *Earth-Centered-Earth-Fixed Frame (E-frame)*, *Navigation Frame (N-frame)* and *Body Frame (B-frame).* The first three are shown in Figure 3.1. Transformations from one frame to another can be found in (Savage, 1998a), (Shin, 2005, pp. 18-28) and (Reinštein, 2011, pp. 35-38).

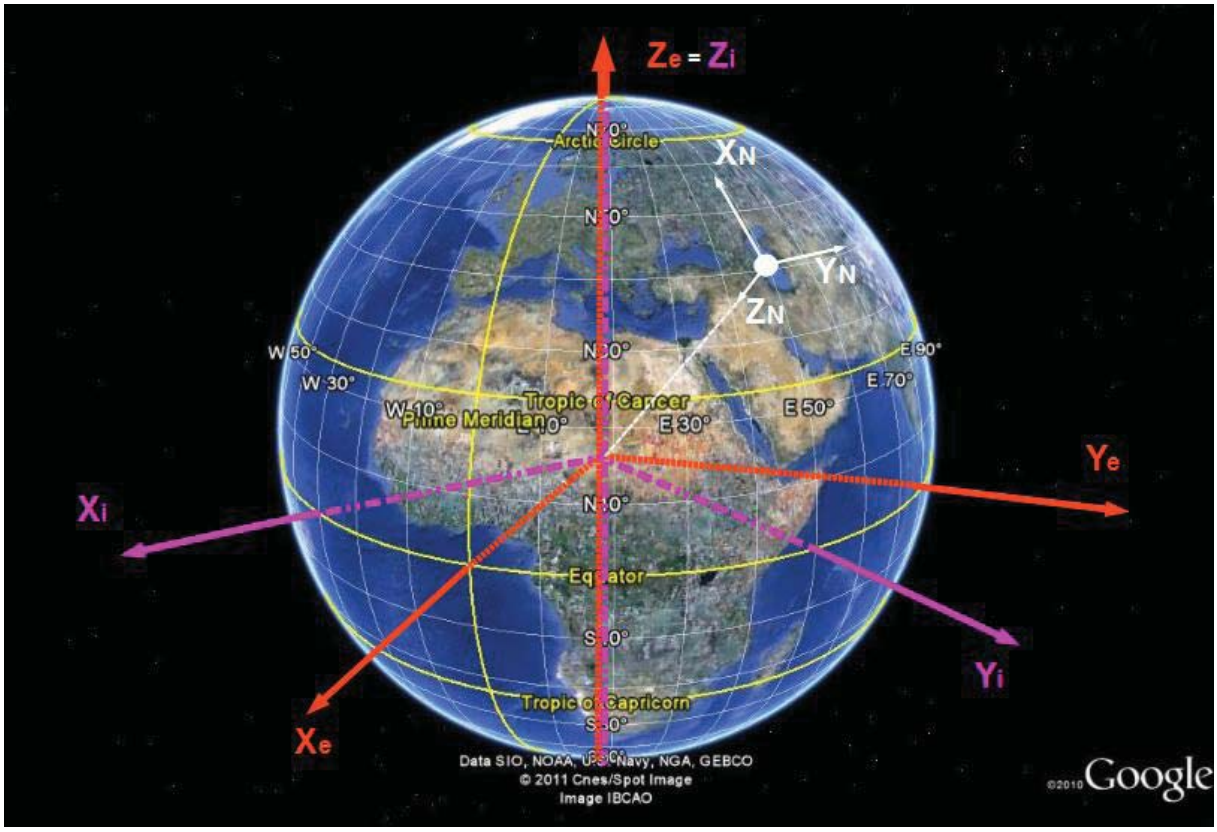

Figure 3.1 I-frame, E-frame and N-frame (based on *Google Earth*)

Earth-Centered Inertial Frame has its origin in the center of the Earth, its ***x*** axis points towards crossing of celestial equator and ecliptic (Shin, 2005, p. 19), ***z*** points towards the North Pole and ***y*** axis completes the orthogonal system. I-frame is considered non-rotating; yet the solar system orbits around the center of the galaxy. Nevertheless, this movement is below the noise level of existing inertial sensors (Reinštein, 2011).

Earth-Centered-Earth-Fixed Frame has its origin in the center of the Earth. Its ***z*** axis is concurrent with the ***z*** axis of the ECI frame, ***x*** points towards the Prime Meridian and ***y*** completes the orthogonal system. Because of the fixation to the Earth, E-frame rotates in the I-frame with the rate of celestial angular rate.

Navigation Frame has its origin in the center of gravity of the navigated object, its ***x*** axis points towards the north, ***y*** points towards the east and ***z*** points toward the center of the Earth. Its position relative to the E-frame is described using ***latitude and longitude*** (Reinštein, 2011).

Body Frame coincides with the spatial frame of the sensor. The ***x*** axis points towards the nose of the vehicle, ***z*** towards the bottom of the vehicle and the ***y*** completes the orthogonal system. It is supposed, that the inertial sensor is aligned with the body of the vehicle.

The mechanization algorithm can be summarized into several steps:

1. *The gravity vector is evaluated based on longitude and latitude using MATLAB exact model*
2. *Inertial data are loaded*
3. *Filter and integration scheme is selected*
4. *Memory space for Euler Angles, DCMs, Quaternions, increments in Euler angles and time vector is reserved*
5. *Filters are applied on the inertial data*
6. *Coarse alignment is performed to evaluate initial Euler angles* (Sotak, 2010)
7. *Set of initial Quaternions and DCM is evaluated*
8. *Attitude Mechanization cycle is launched and repeated for the whole data set*
    a. *One step of mechanization of gyroscopes is performed*
        i. *Additions to Euler angle is evaluated based on selected integration scheme*
        ii. *Frame rotation vector is evaluated*
        iii. *Quaternion from B-frame in time **k** to B-frame in time **k+1** is evaluated* (Shin, 2005)
        iv. *Quaternion from B-frame in time **k** to N-frame in time **k** is evaluated* (Shin, 2005)
        v. *Euler angles and DCM are extracted and saved*
    b. *One step of mechanization of accelerometers is performed*
        i. *Initial offset is subtracted*
        ii. *Low order Moving Average filter is applied*
        iii. *Coarse alignment is performed* (Sotak, 2010)
        iv. *Euler angles are stored separately from the ones from gyroscope mechanization*
9. *Euler angles are plotted and RMS error is computed comparing the result to the reference*

4 RESULTS AND EVALUATION

4.1 ALLAN VARIANCE ANALYSIS

The main goal of the AVAR analysis is to provide data for future work. Identified noise terms can be used to create a mathematical model of the sensor. This model can subsequently be used for the Kalman filter (Reinštein, 2011), (Shin, 2005). Nevertheless, Kalman filter is not part of this work. The measurement of the ADIS16405 data took approximately 1.3 hours with a sampling frequency of **231.5859 Hz**. This unusual value was a result of the fact that development board ADISUSB and supplied software did not allow setting of the exact sampling frequency. Because of this, the sampling frequency had to be evaluated after the measurement by dividing the number of samples by the measurement duration, which was indicated by the software. Along with the accelerometer and gyroscope data, temperature of the sensor was measured, see Figure 4.1. It changed only by 1.5°C, hence taking into account the operating temperature range of -40°C to 105°C, it could be considered constant. The sensor was positioned on a soft foam pad lying on a massive marble sill; therefore all significant vibrations were expected to be dampened and only sensor noise to be measured. For the AVAR evaluation, a MATLAB function **allan.m** (Hopcroft, 2010) was used.

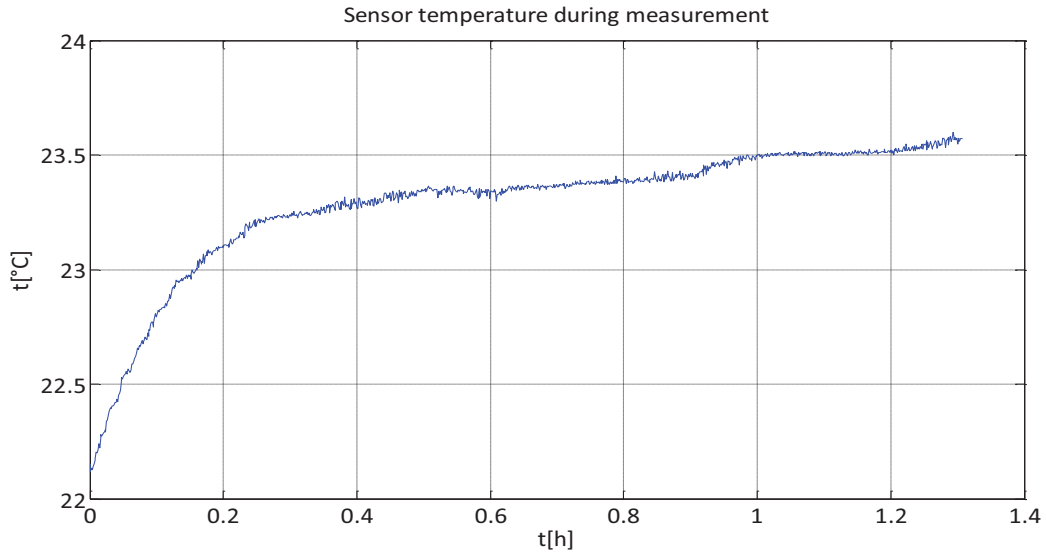

Figure 4.1 Sensor temperature development during measurement

An example of the AVAR logarithmical plot is shown in Figure 4.2. The rest of the evaluated AVAR plots are shown in ***Annex A.*** According to Figure 2.8 and Table 2.1, slopes of corresponding noise terms were identified and various noise term parameters were evaluated. A summary of all of them is shown in Table 4.1 and Table 4.2. The given measurement errors were evaluated using formula (El-Sheimy, Hou, & Niu, 2008, p. 144):

$$\sigma(\delta) = \frac{1}{\sqrt{2(\frac{N}{n} - 1)}} \tag{4.1}$$

where ***σ(δ)*** is the percentage error, ***N*** total number of samples and ***n*** number of samples in a data cluster corresponding to the averaging time.

Comparing the measured AVAR of gyroscopes (Figures A.4-6) and Figure 4.4 supplied by Analog Devices, it was possible to say that they were accordant. There were differences for ***τ > 100s***, but with regard to the measurement error, this difference was not found important. Datasheet noise term parameters of the gyroscopes and the measured noise term parameters were in accordance. The nominal *Bias Instability* is 0.007 °/s = 25.2 °/h. The measured one varied from 33 to 54°/h and with respect to that Analog Devices did not specify the error of their measurement, the values were expected to overlap. Nominal *Angular Random Walk* is 2°/$h^{1/2}$ and it corresponded to the measured ones. However, the manufacturer did not mention any other terms, yet gyroscopes X and Y embodied *Rate Random Walk.*

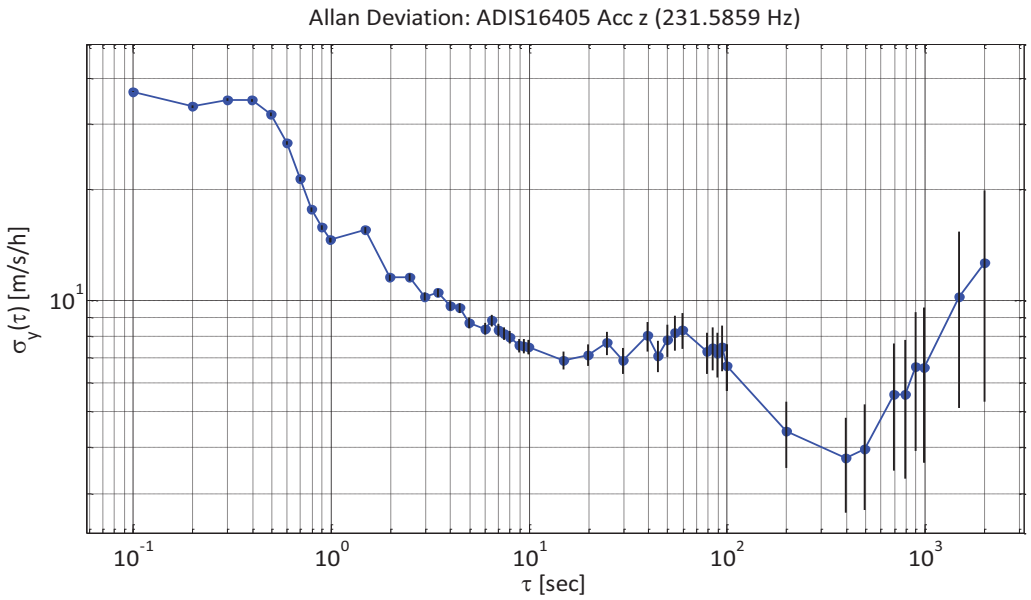

Figure 4.2 Example of the Root AVAR logarithmical plot (Accelerometer z)

Noise terms of accelerometer signal of ADIS16405			
Axis	Quantization noise [m/s]	Velocity random walk [m/s/$h^{1/2}$]	Bias instability [m/s/h]
X	0.0010630 ± 0.0000098	0.587 ± 0.019	10.05 ± 0.57
Y	0.0022030 ± 0.0000022	0.370 ± 0.012	9.66 ± 0.55
Z	0.002439 ± 0.000025	0.341 ± 0.011	11.3 ± 1.1
Axis	Rate random walk [m/s/h/$h^{1/2}$]		Drift rate ramp [m/s/h^2]
X	149 ± 12		/
Y	/		87 ± 42
Z	/		36 ± 17

Table 4.1 AVAR noise terms of accelerometer signal

Comparing Root AVAR of the accelerometers in Figure 4.5 and the measured ones (example Figure 4.3), the graphs were slightly different. The manufacturer one showed only *Velocity Random Wa*lk and *Bias Instability.* The measured data contained also significant *Quantization Noise, Rate Random Walk* and *Drift Rate Ramp* (however, last two are in averaging times with high percentage error).

The value of *Bias Instability* specified by manufacturer was *0.2 mg = 7.1 m/s/h*. The measured values were slightly higher. The nominal *Velocity Random Walk* was mentioned in the datasheet: *0.2 m/s/h$^{1/2}$*. This value was in accordance with the measured ones, which were higher by several tenths. It is necessary to state that manufacturer did not mention any errors; hence, the values might overlap as well.

Measured *Quantization Noise* was found in all three signals and with respect to the consistency of values, it was considered correct.

Noise terms of gyroscope signal of ADIS16405			
Axis	Quantization noise [°/s]	Angle random walk [°/h$^{1/2}$]	Bias instability [°/h]
X	/	2.029 ± 0.063	33.1 ± 3.4
Y	/	1.783 ± 0.047	46.6 ± 3.6
Z	/	4.39 ± 0.10	54 ± 13
Axis	Rate random walk [°/h/h$^{1/2}$]		Drift rate ramp [°/h^2]
X	/		/
Y	340 ± 160		/
Z	/		/

Table 4.2 AVAR noise terms of gyroscope signal

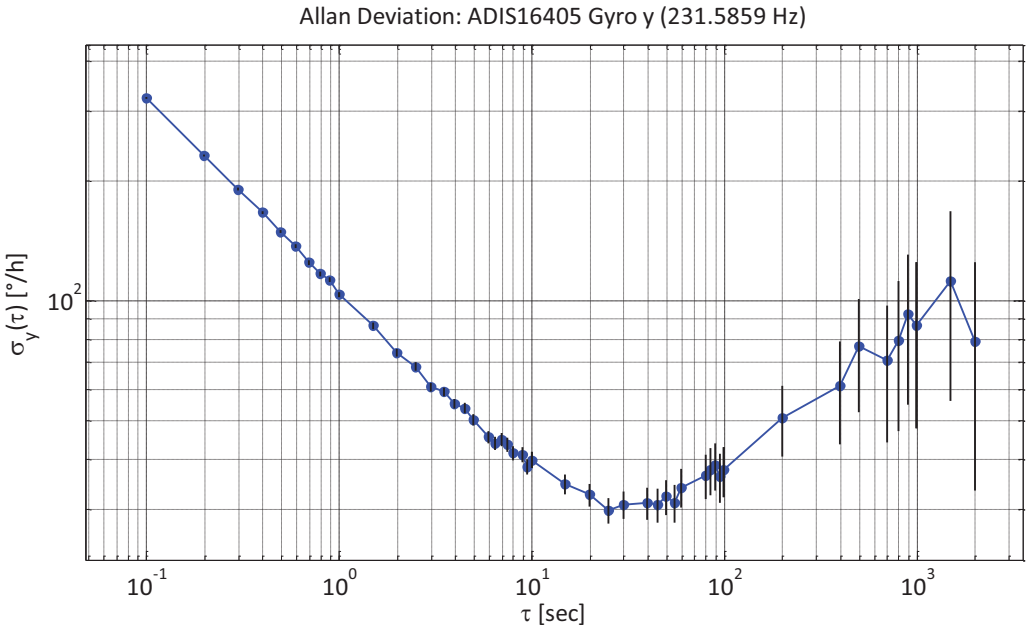

Figure 4.3 Example of the Root AVAR logarithmical plot (Gyroscope y)

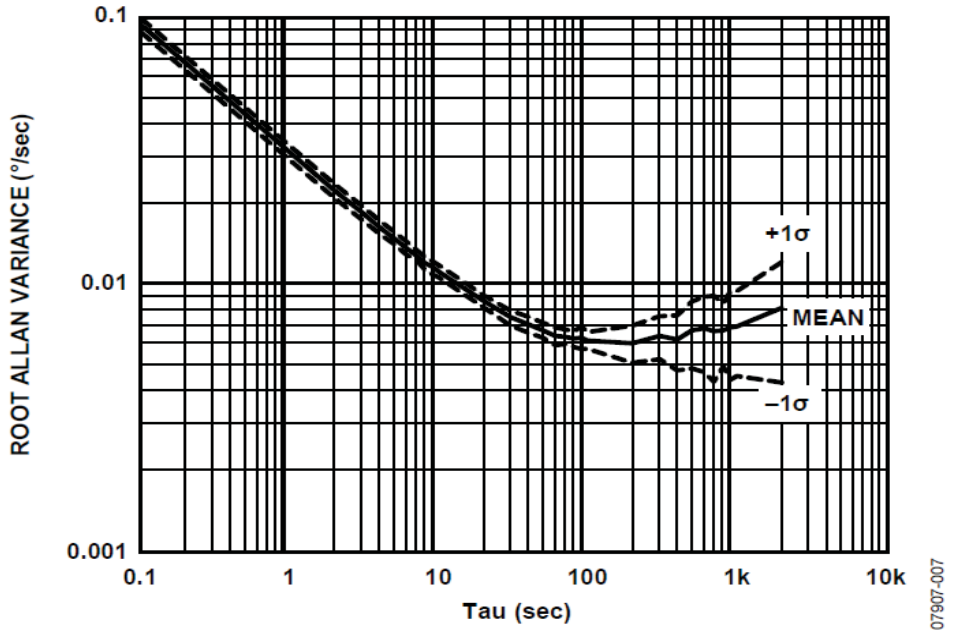

Figure 4.4 Gyroscope Root AVAR according to (Analog Devices, 2009)

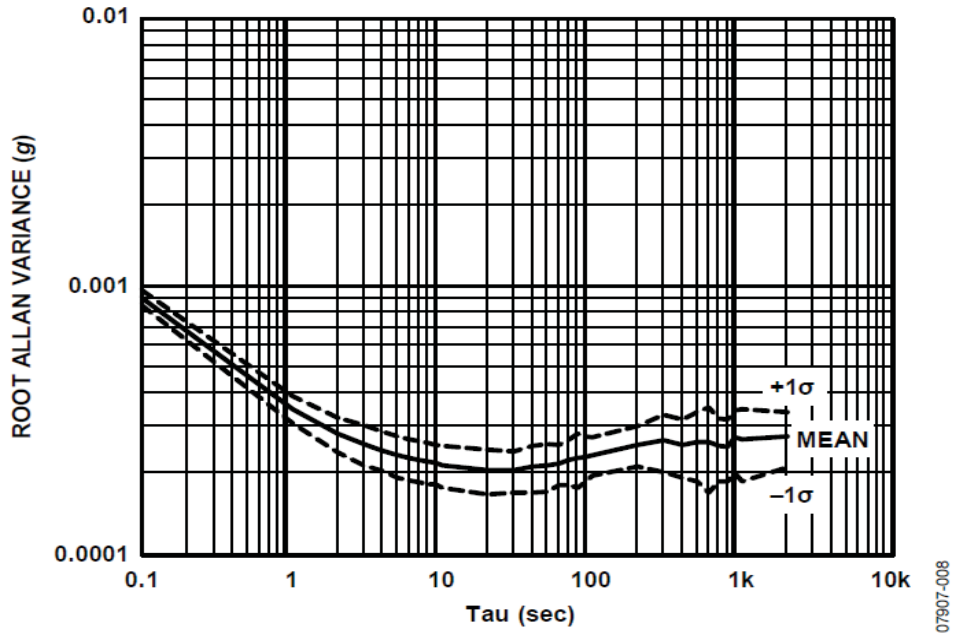

Figure 4.5 Accelerometer Root AVAR according to (Analog Devices, 2009)

4.2 VIBRATION ANALYSIS AND FILTER DESIGN

To analyze possible vibrations, experimental solution was proposed. The RC model Bellanca Super DecathlonXXL was equipped with MVVS 58S motor with maximal 6700 RPM. Thus, the expected target frequency should have been around 111 Hz (701 rad/s). A small electromotor with an eccentric balance wheel originally embedded in a cellular phone was used. To control its RPM, an evaluation board with STM32 ARM Cortex M3 microcontroller was used as a PWM (Pulse Width Modulation) regulator (Figure 4.6). It was first set to change power in steps long approximately one second so the recorded signal from inertial sensors could be easily analyzed.

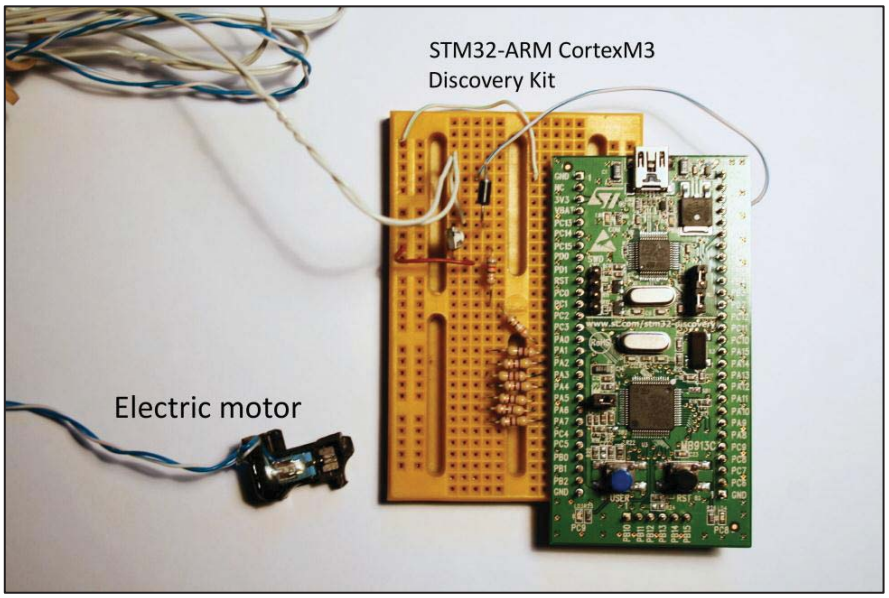

Figure 4.6 Motor with an eccentric wheel and PWM regulator

The sensor was mounted on a soft pad and the motor was attached to the sensor board by rubber bands (Figure 4.8). The motor was positioned in several ways, the one with the largest impact to the signal was subsequently chosen. The resulting spectrum was composed of harmonic components with frequencies from 40Hz to 110Hz (Figure 4.7). This was a satisfying result, the range of PWM regulator did not need to be changed (the goal was top frequency 110 Hz of the real motor). Only the time development was changed from one-second steps to a continuous linear change from minimum to maximum power and back. This was supposed to simulate conditions in real aircraft, where pilot changes thrust and the vibrations change as well. Also, this approach prevented Moving Average filter to be favored (because of its capability to perfectly suppress one selected harmonic signal).

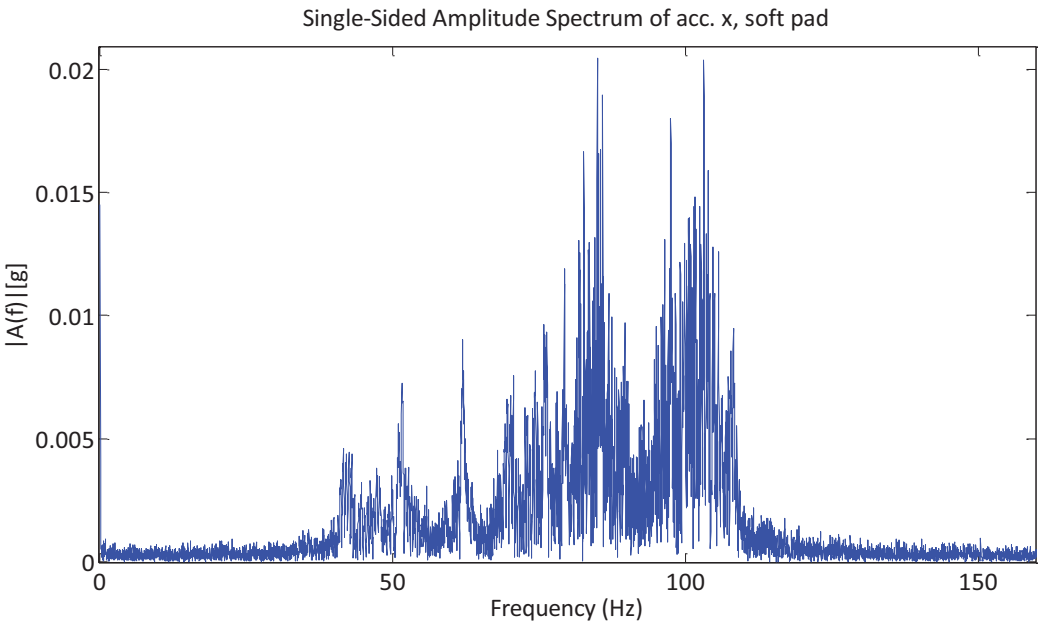

Figure 4.7 Spectrum of vibrations (el. motor), accelerometer x [g]

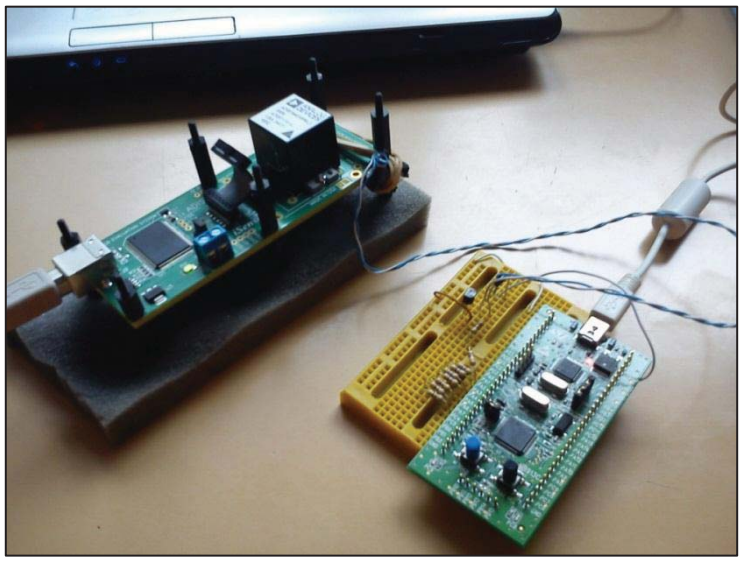

Figure 4.8 Setup for recording of inertial signals with vibrations (the motor attached to the evaluation board)

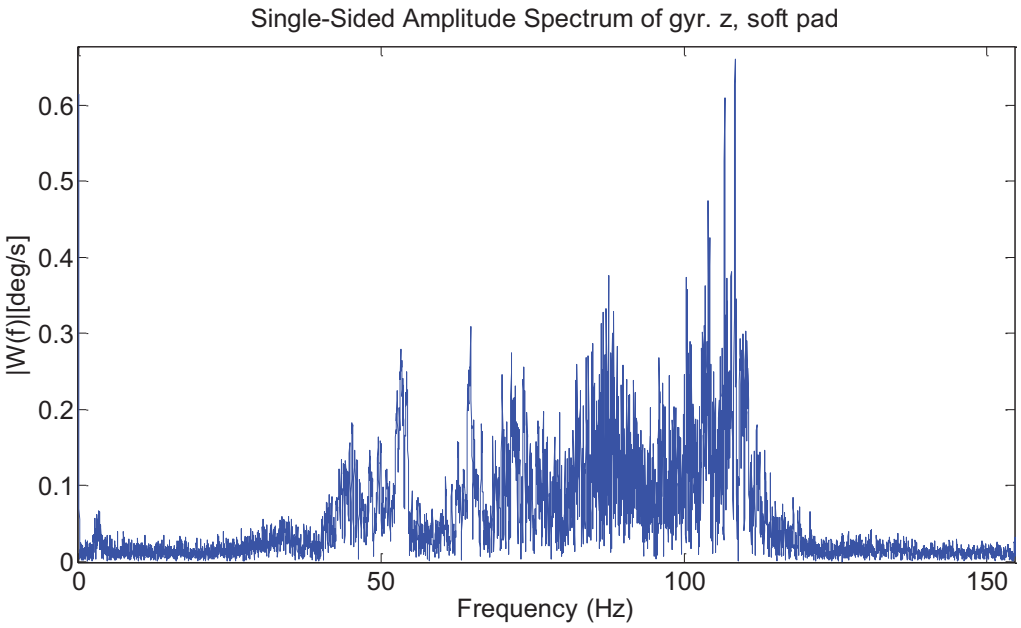

Figure 4.9 Spectrum of vibrations (el. motor), gyroscope z [deg/s]

With the source of the vibrations prepared and tested, the sensor was attached to the calibration table RoTiP. First, measurements without any movement were performed (Figure 4.10).

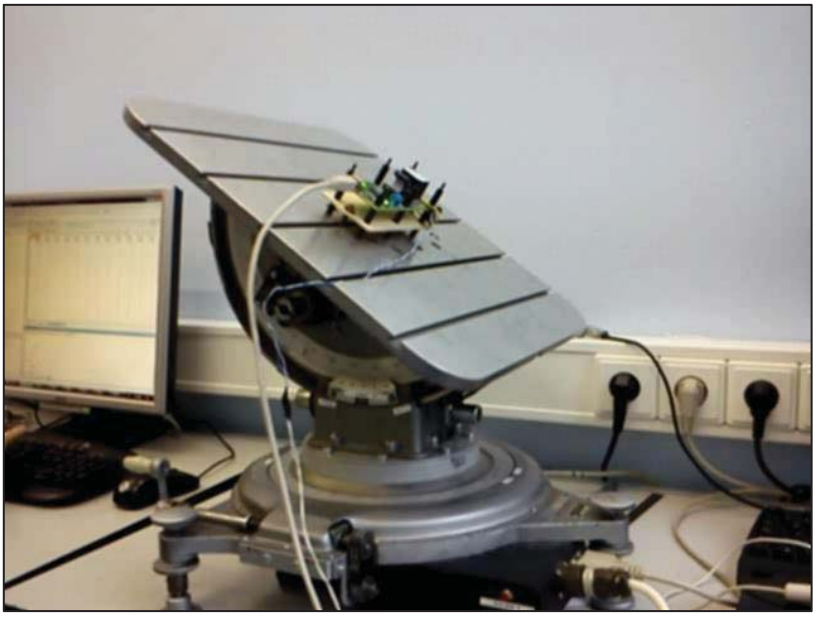

Figure 4.10 Sensor attached to the RoTiP

The resulting spectrum changed, the solid fixation to the calibration table dampened the vibrations by one decade and shifted the harmonics to the range of approximately 75Hz to 150Hz. This has shown that the mounting is one of the vital aspects of the final performance of the system. Two examples of the spectrum are plotted in Figure 4.11 and Figure 4.12. Also, a disturbing fact was found in the signal of the gyroscopes – the signal spectrum covered all frequencies from 0 Hz to 150 Hz. This complicated the filter design, because it was necessary to preserve lower frequencies containing the useful signal. The subsequent measurement showed, that useful signal has much higher ampli-

tude (rotation of 10 deg/s = 0.175 rad/s has magnitude two decades higher than considered vibrations.)

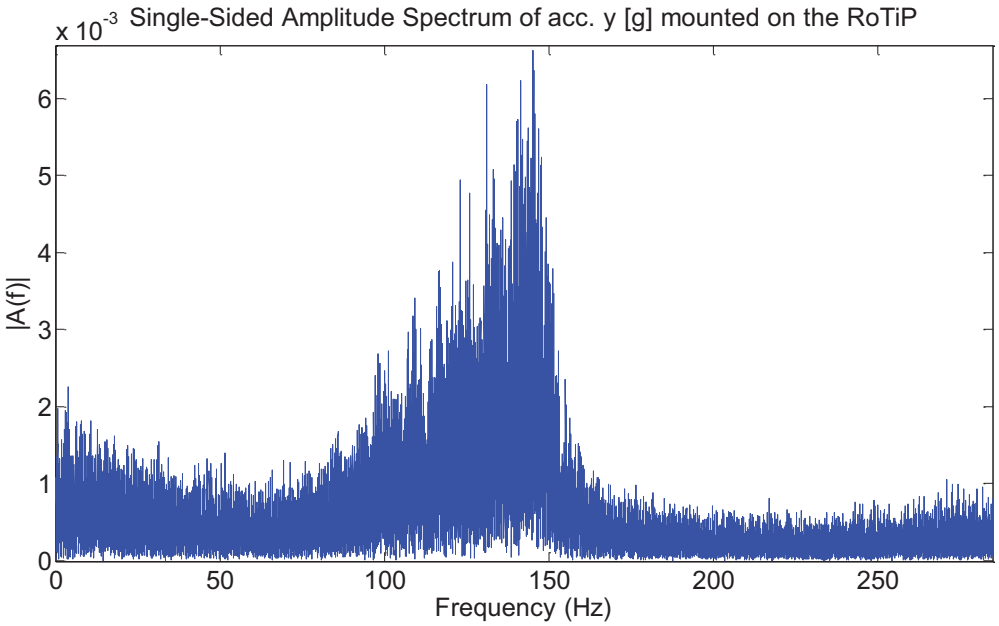

Figure 4.11 The spectrum of the accelerometer x after mounting on the RoTiP

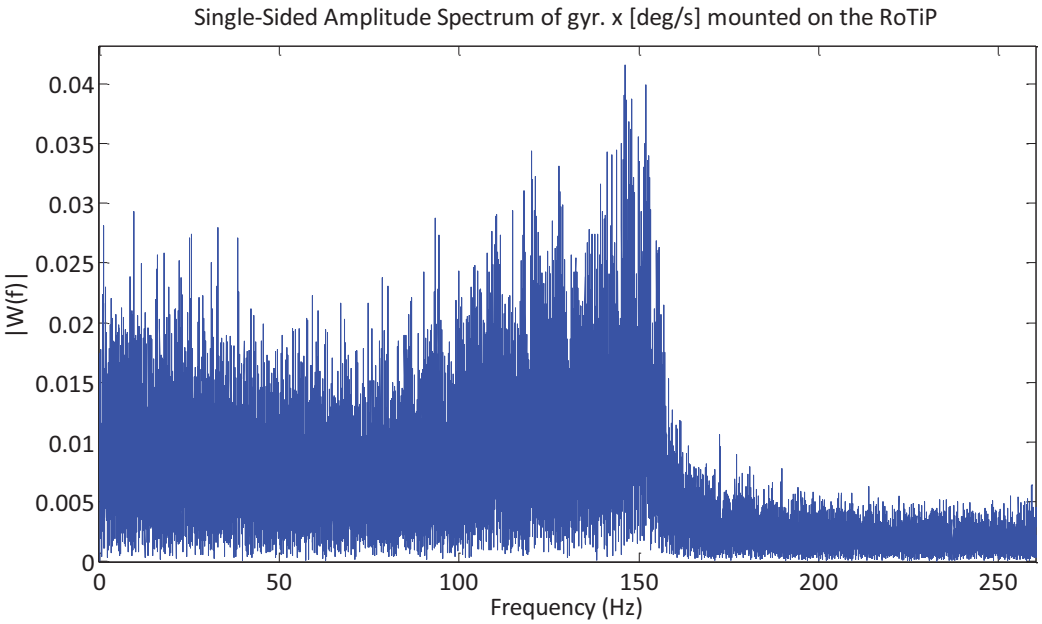

Figure 4.12 The spectrum of the gyroscope x after mounting on the RoTiP

Based on these measurements a set of filters was designed. All of them were designed or naturally behaved as low-pass filters; their parameters are shown in Table 4.3. The slope of the amplitude part of the transfer function at the nominal frequency was selected in such a way to not overpass the order of FIR filter of 150. The reason was to prevent high signal delay. At the sampling frequency of approximately 320 Hz this caused maximum delay of 0.5 second.

Filter Type	Nominal Parameters	Setting				
		#1	#2	#3	#4	#5
FIR	freq. pass/stop [Hz]	4/10	6/14	16/24	26/34	36/44
IIR	freq. pass/stop [Hz]	4/10	6/14	16/24	26/34	36/44
Wavelet	**wden** parameters	Thresholding selection rule = **minimaxi**, Thresh. type = **hard**, **No thresh. rescaling**, Wavelet = **Daubechies 8** , decomposition level = **6**				
Moving Average	Filter order	10	50	100	200	300

Table 4.3 Designed filters

The selection of filer frequencies was based on the presumption that the lower frequencies would affect the navigation more than the higher ones, because of the presence of integration in the Attitude mechanization. The intention was to find an acceptable bound of the dynamics and set the filter stop frequency as close as possible because of the wide-band character of the measured vibrations. This concerned FIR, IIR and MA filters design. The wavelet method was set to a maximum decomposition level in accordance with preliminary experiments using the Wavelet toolbox GUI, which was able to show spectral composition of the filtered *details*. With the setting of decomposition level to 6, displayed spectrum was the most resembling to the measured one. The type of wavelet was chosen according to the paper (Abdel-Hamid, 2005, p. 94), while it showed a good behavior during the GUI design.

After designing the filters, two experiments were performed: the first using the RoTiP and its capability to create a reference log of the Euler angles; the second with the RC aircraft model. The one containing the calibration table was intended for dynamic evaluation of the filtering methods, the second to record real vibrations caused by a combustion motor.

The experiment with the RoTiP (Figure 4.13) was prepared as three motions around each axis separately, at angular rate of 10 degrees per second. The calibration table first performed a roll rotation of 40 degrees, then returned to the default position, then performed a pitch rotation of 20 degrees and returned to the default position and finally changed the yaw angle to 60 degrees and back to 0 degrees. The signal was measured with and without vibrations, with approximate sampling frequency of 320 Hz (which was found sufficient because of the maximum vibration frequency of 150 Hz).

The second experiment concerning the RC model (Figure 4.14) was performed during motor testing. The data were collected while the plane was steady on the ground. Unfortunately, there was no possibility of obtaining referential attitude angles. Hence, after the initial alignment of the body frame during mechanization, its attitude was expected to be constant. The sensor was attached to the model as showed in Figure 4.15. The RC model was tested without its wings; therefore a slight change in its dynamics was expected. This was confirmed during the test, when the RC model was vulnerable to roll motion; the sensor also captured this motion in the gyroscope **y** signal.

There were four measurements: first two measuring accelerometer and gyroscope separately in order to achieve maximum sampling frequency and two measurements for gathering complete sets of inertial signal for the mechanization.

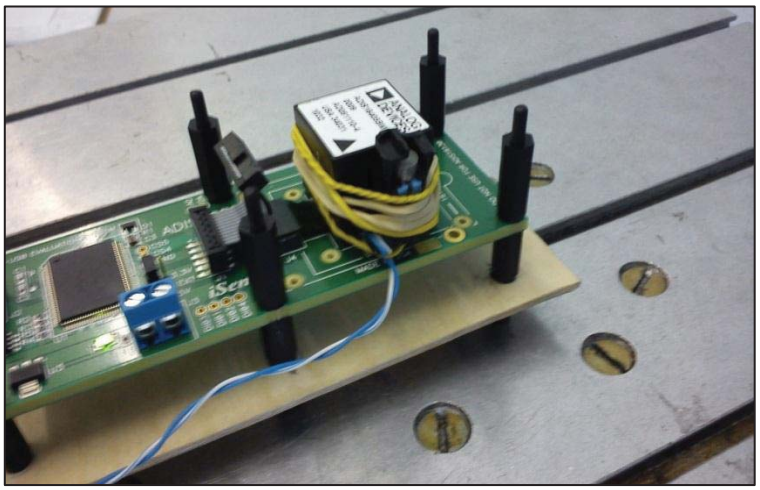

Figure 4.13 The sensor attachment to the RoTiP

Figure 4.14 RC model of Bellanca Super Decathlon with ADIS16405 onboard

One of the last two measurements was longer and a thrust of the motor was being changed to cover a variety of RPMs. The second one was shorter with the motor set to a high speed. See figures Figure 4.16, Figure 4.17, Figure 4.18 and Figure 4.19, where selected spectra are shown. The main difference from the experimental source of vibrations was the magnitude of the vibrations. It is important to mention that the units of these graphs are [rad/s] and [m/s^2] diverging from the preceding graphs, because of the mechanization. The bandwidth of the vibrations spectrum was similar to the simulated one (by the electric motor) and therefore the designed filters could be used.

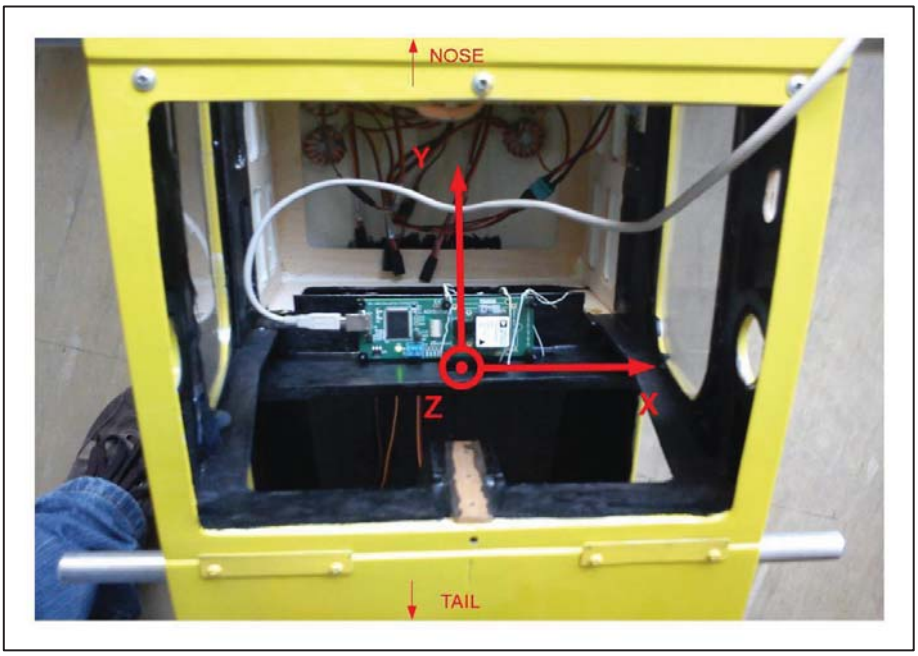

Figure 4.15 Sensor attachment to the model chassis (spatial frame of the sensor displayed)

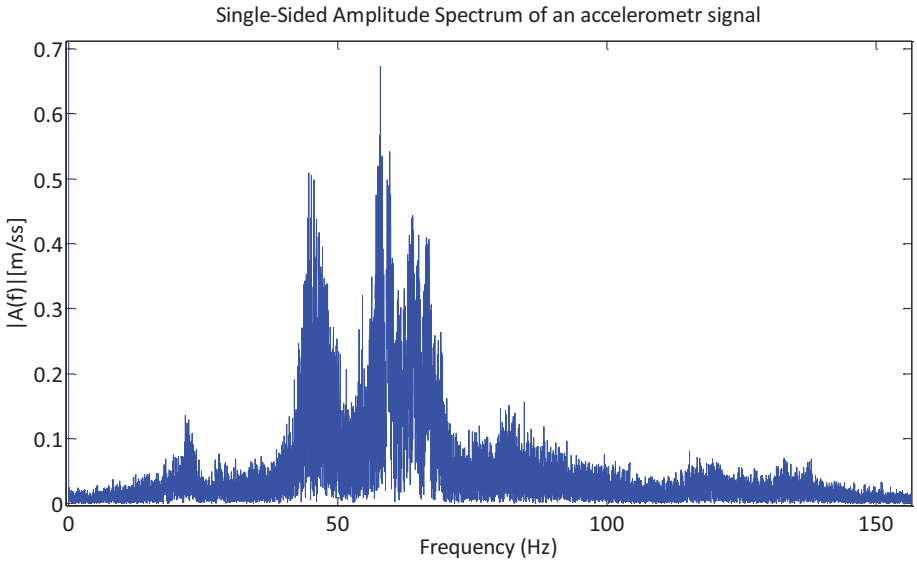

Figure 4.16 An accelerometer signal spectrum during RC model test, varying thrust

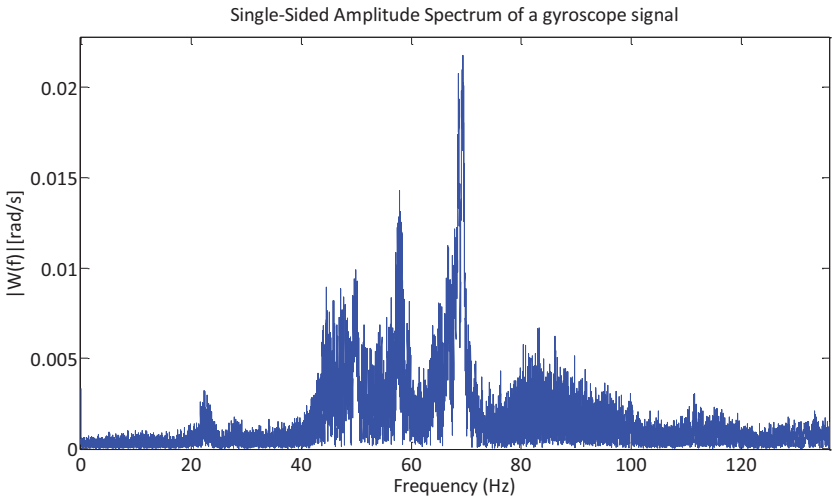

Figure 4.17 A gyroscope signal spectrum during RC model test, varying thrust

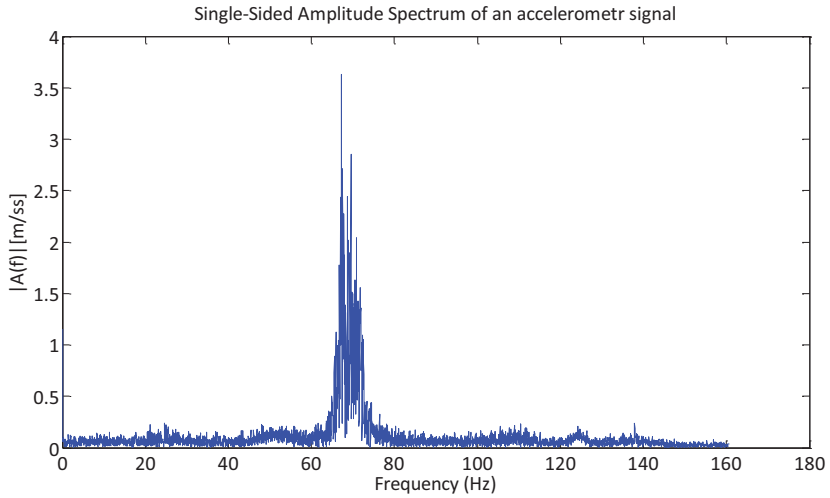

Figure 4.18 An accelerometer signal with motor at high RPM

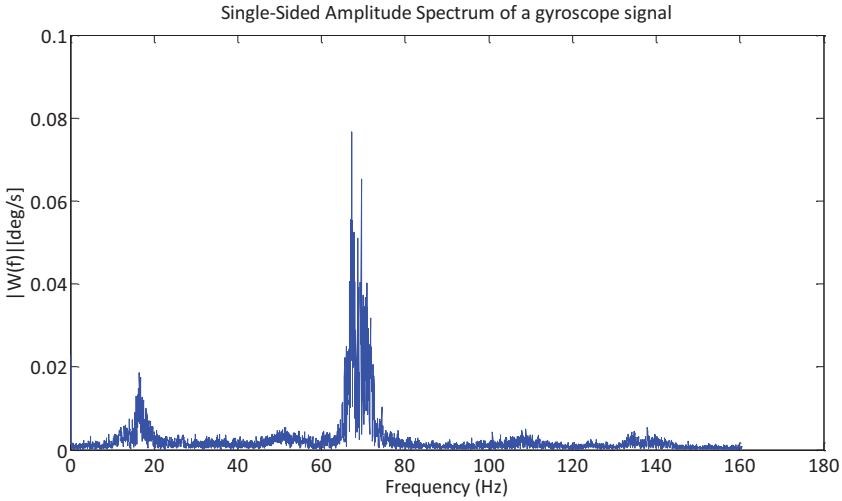

Figure 4.19 A gyroscope signal with motor at high RPM with a peak at 16 Hz caused by a lack of wings (roll movement)

4.3 FILTER PERFORMANCE VERIFICATION

With the data and filters prepared, a series of mechanizations were performed to select the most suitable filter. The attitude mechanization mentioned in Chapter 3 was utilized. In the end of the mechanization, RMS of the total error was evaluated. The error was considered the difference between indicated attitude and the reference. The measurements performed on the calibration table were referenced by the table output; the measurement with the RC model did not have any reference. This problem was solved by observing the attitude mechanization development of the RoTiP measurements. While the mechanization of the gyroscope signals tended to drift away, attitude computed using coarse alignment was almost identical with the reference in the steady parts of the measurements (while the table was not moving). Therefore, initial alignment computed from the accelerometers signal was taken as a reference for the whole measurement. Because of this, there is a potential of a deviated results for the RC model measurements; yet only biased. For a comparison among them, this method was sufficient. The example of the attitude mechanization is shown in Figure 4.20 and Figure 4.21. Also, the geometry of the task does not allow yaw angle evaluation based on the coarse alignment. Therefore, it is not included in the RMS evaluation.

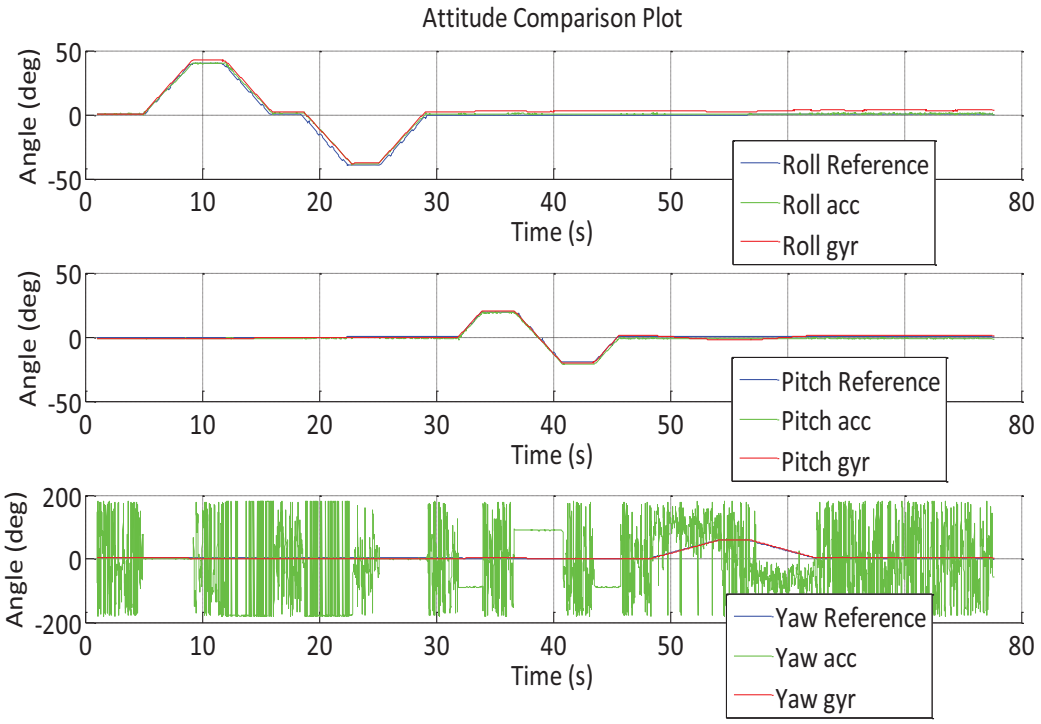

Figure 4.20 Attitude mechanization of the inertial data (RoTiP, no vibration, no filtration)

Before comparing the effects of the filters, two important aspects had to be examined. The first was the influence of deterministic errors. The algorithm contains a section, where calibration matrices were applied. A calibration matrix was obtained by a Thin-Shell algorithm (Šipoš, 2010) applied on a multi-position calibration data. The effect of this matrix was compared to a unit matrix corresponding to no calibration with the difference in result of 0.1 degree. This difference was found

much smaller than the error caused by noise and vibration, thus the calibration of the data realized in the final version of the algorithm and the deterministic errors of ADIS16405 were neglected.

The second aspect was the integration scheme. Because the integration of a periodical signal over one period is equal to zero, it was expected to improve the overall performance. However, the digital approach required selection of some integration approximation. Two approaches were examined:

The rectangular rule which computes an increment in time *k* simply as a gyroscope signal in time *k* multiplied by a sampling period

The trapezoidal rule, for which an increment in time *k* is equal to *0.5*(GYR(:,k-1) + GYR(:,k))*Ts* (i.e. an average from last two gyroscope signal samples multiplied by a sampling period).

These schemes were compared by mechanization of a signal containing vibrations without using any filter. The differences were not greater than 0.2° and no trend was observed. Thus, a trapezoidal rule was selected and used for all further computations. The important fact is the sampling frequency. All measurements taken with ADIS16405 were at 300 Hz and higher; the additional measurement taken onboard a real aircraft during flight (but using 3DM-GX2 MicroStrain for practical reasons) was sampled at 100 Hz. This relatively high frequency may have hidden the difference between these two schemes. For lower sampling frequencies, greater difference might be observed.

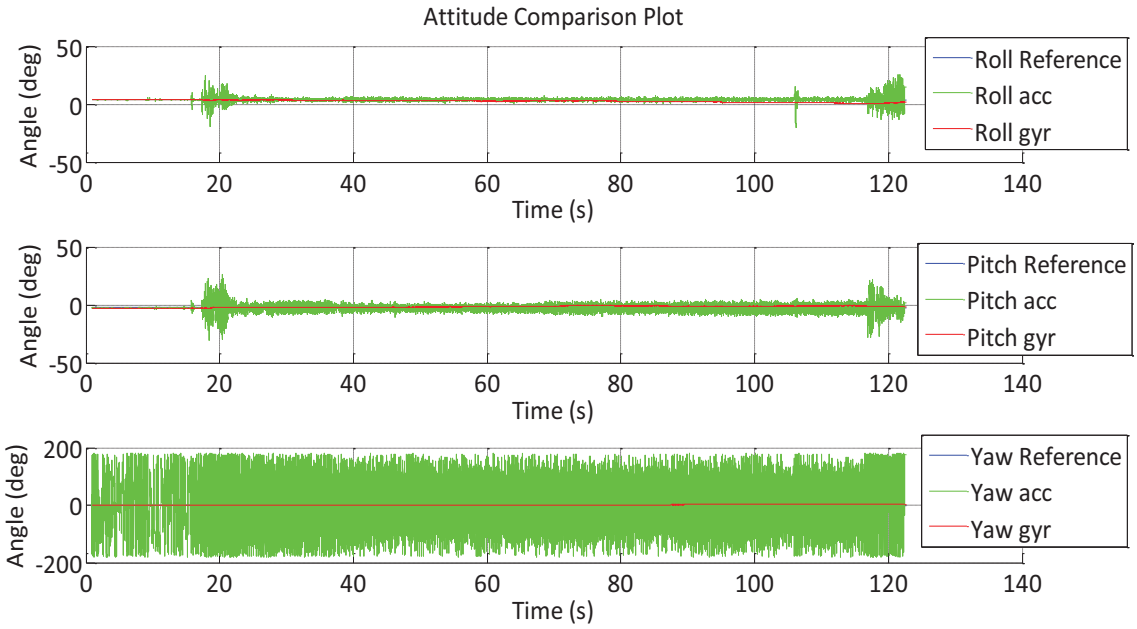

Figure 4.21 Attitude mechanization of the inertial data (RC model, vibrations, no filtration)

After investigating calibration impact and the integration scheme, all filters were compared by mechanization of four inertial measurements: two originating from RoTiP measurements and two already mentioned RC model measurements. The results are shown in Figure 4.22, Figure 4.23, Figure 4.24 and Figure 4.25. While the first two tables may be disappointing (the best result is the one without any filter) it is necessary to say the result was expected. The first measurement was without vibrations; thus the filter could only diminish the overall performance (partly because its stop fre-

quency may interfere with the frequencies of the dynamics of the experiment, partly because of the non-flat pass part of the filter transfer function). The second measurement contained vibrations but they were dampened by the attachment, hence the second measurement could be also considered without vibrations. Therefore, the positive effects of the filters were more visible in the last two measurements with the RC model.

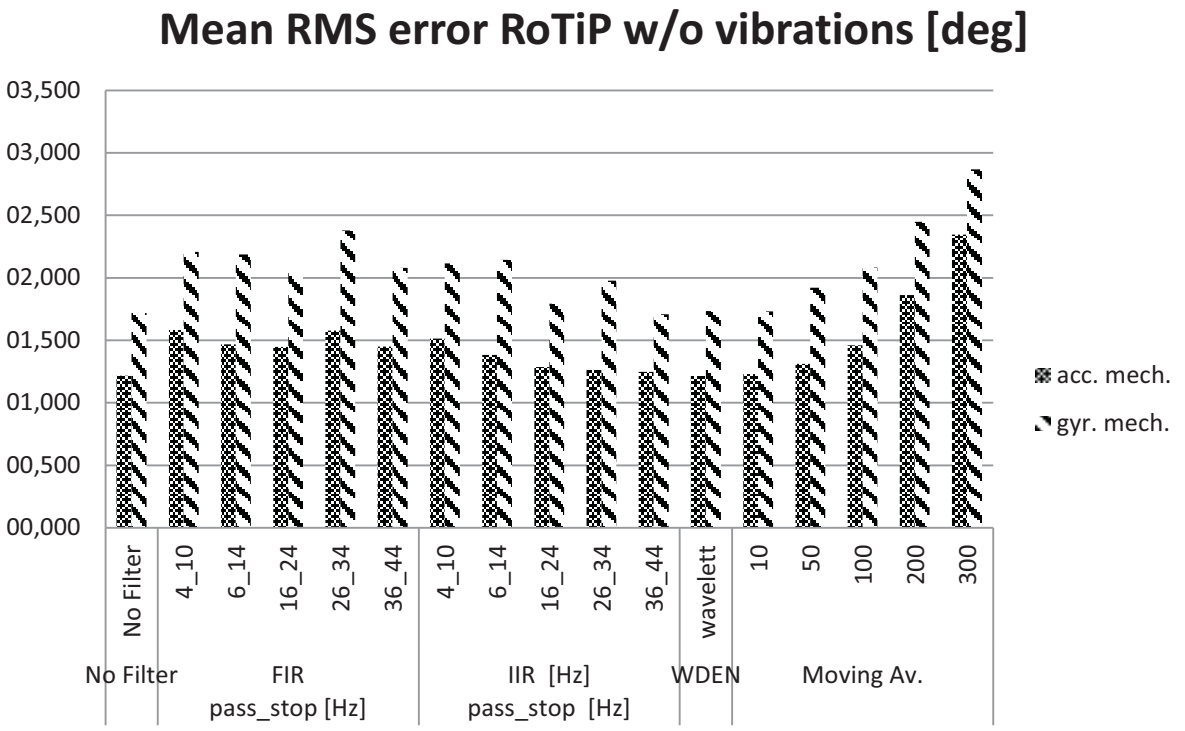

Figure 4.22 Filter performance comparison, RoTiP measurement without vibrations; the mean of RMS errors of the gyroscopes and accelerometers based mechanization is displayed separately for each filter. The Yaw evaluated from accelerometers signal is ignored.

Because of the character of this experiment discussed above, the first two measurements could be taken as criterion for dynamics preservation, the second two as criterion for vibration damping. Filters with good results were the IIR and FIR filters with cut-off frequencies at 6-14Hz and 16-24Hz respectively, because they preserved dynamics and still dampened the vibrations. However, the effect of the filters was more visible for the accelerometer mechanization, because at each step, the attitude was computed from the actual accelerometer signal. The gyroscope mechanization contained integration of the signal; therefore the effect of filtering was less apparent (not taking in account those filters actually deteriorating the navigation accuracy). The other observation was that the moving average filter has shown good results for the accelerometer mechanization. It might be reasonable to filter the gyroscope signal by the proposed IIR or FIR filter and the accelerometer signal by the moving average of order of 100, which has shown good performance both for the dynamics preservation and vibration dampening.

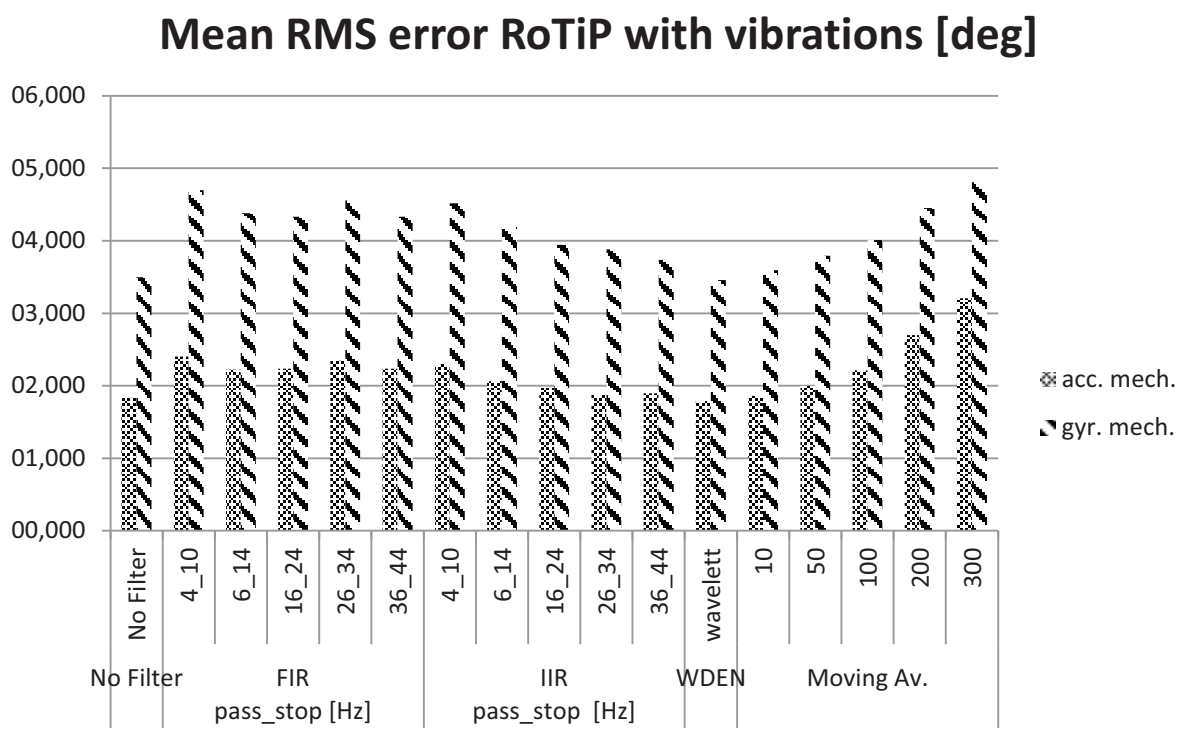

Figure 4.23 Filter performance comparison, RoTiP measurement with vibrations; the mean of RMS errors of the gyroscopes and accelerometers based mechanization is displayed separately for each filter. The Yaw evaluated from accelerometers signal is ignored.

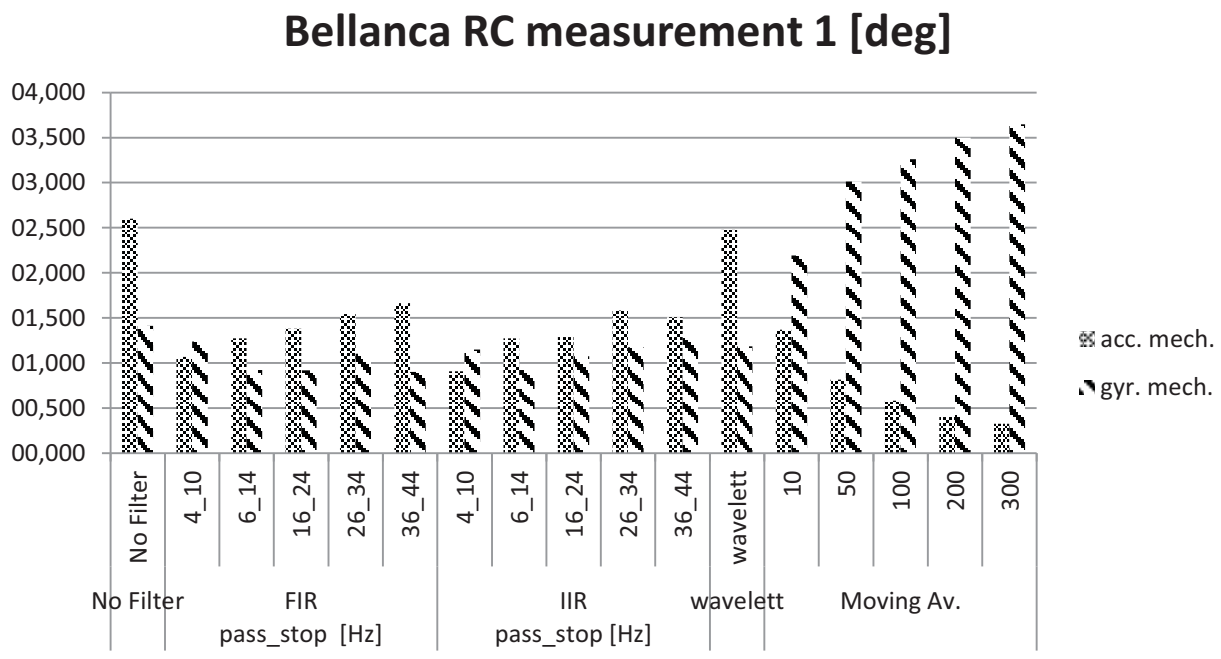

Figure 4.24 Filter performance comparison, RC model measurement (varying thrust); the mean of RMS errors of the gyroscopes and accelerometers based mechanization is displayed separately for each filter. The Yaw evaluated from accelerometers signal is ignored.

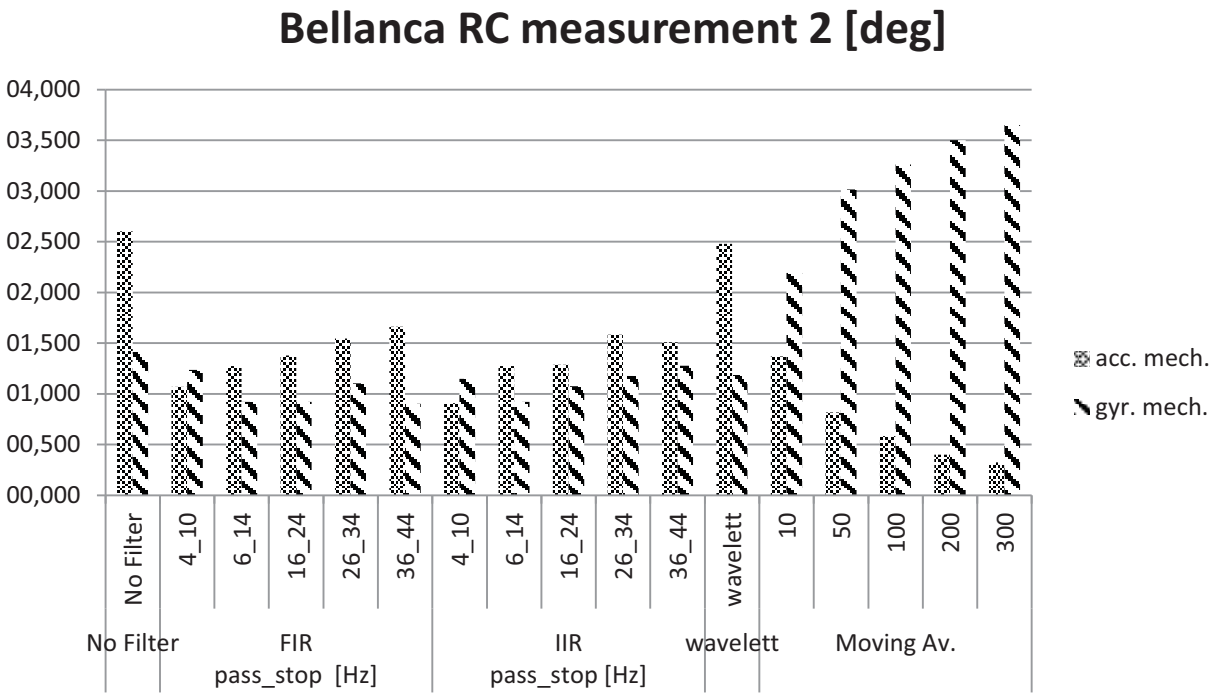

Figure 4.25 Filter performance comparison, RC model measurement (constant thrust); the mean of RMS errors of the gyroscopes and accelerometers based mechanization is displayed separately for each filter. The Yaw evaluated from accelerometers signal is ignored.

To further study the behavior of the proposed attitude mechanization, inertial data recorded using the 3DM-GX2 MicroStrain attitude and heading reference system (AHRS) during real aircraft flight were used for attitude mechanization to observe long-term development. The flight took approximately 35 minutes and there were also reference data; nevertheless, this reference originated from the same inertial sensor, which performed its own attitude mechanization. There are known issues with its magnetometer aiding measurement, thus the reference has to be considered deviated. For this reason, the reference attitude data were taken as a rough approximation of the real values. The attitude mechanization without any filters is shown in Figure 4.26 and in detail in Figure 4.27. The observation confirmed sensitivity of the accelerometer mechanization to the vibrations and revealed a trend of the gyroscope mechanization to drift away as well as the fact that the mean value of the accelerometer mechanization attitude tended to keep a constant error.

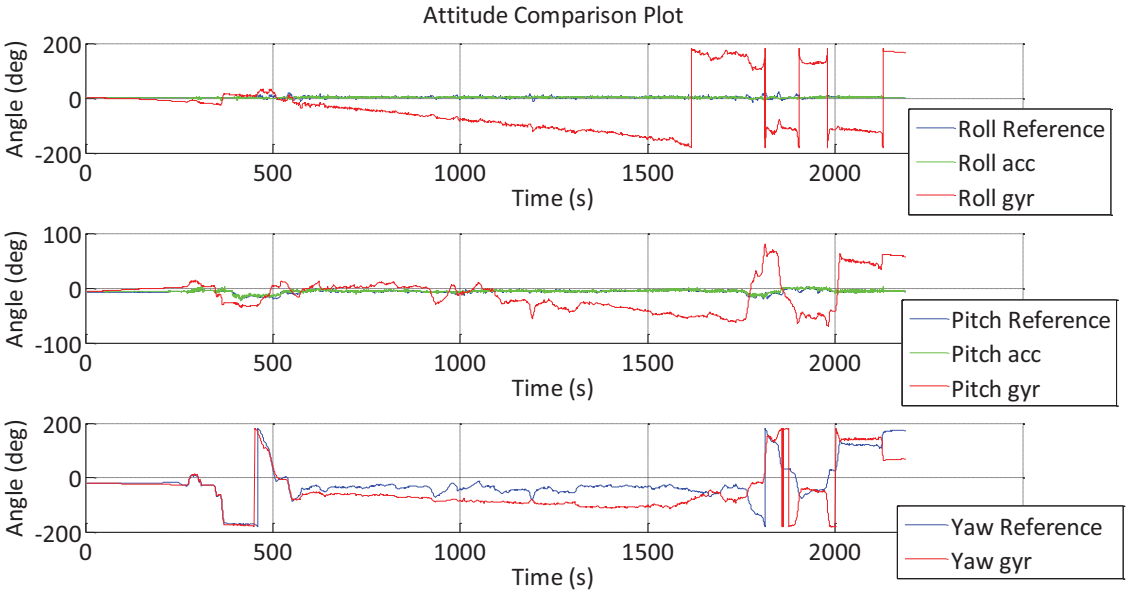

Figure 4.26 Real flight data attitude mechanization (MicroStrain)

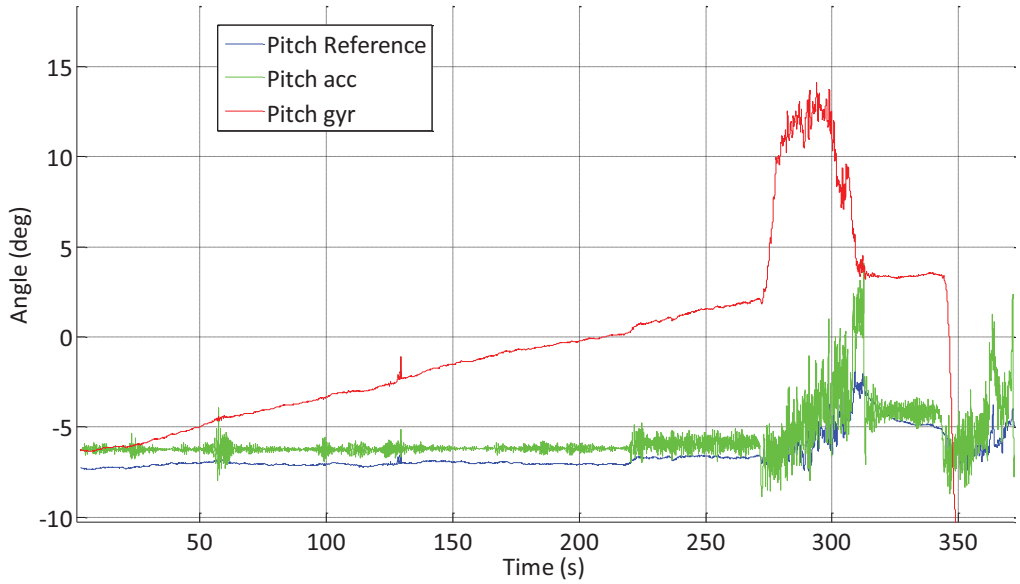

Figure 4.27 Pitch angle mechanization detail (Real flight data, sensor MicroStrain)

Based on the observation, a possibility of dealing with the gyroscope mechanization drift by using the accelerometer computed attitude as a low-frequency reference for corrections was proposed. We suggested a feedback which would take into account the difference between these two mechanizations to correct the gyroscope mechanization. This solution is discussed in the next chapter.

4.4 Gyroscope Mechanization Correction Feedback

The real-data long term mechanization showed that the gyroscope mechanization has been less sensitive to vibrations yet has tended to drift with time. The coarse alignment was less accurate if vibrations were present and of course if the sum of all specific forces was not equal to the gravitational acceleration. Also, the accelerometer mechanization was only able to determine pitch and roll angles from the nature of the task.

A solution was proposed: a difference between gyroscope and accelerometer evaluated pitch and roll angles would be evaluated, processed and provided to gyroscope signal integration as a feedback, which prevented gyroscope mechanization from drifting. The block diagram describing this procedure is shown in Figure 4.28.

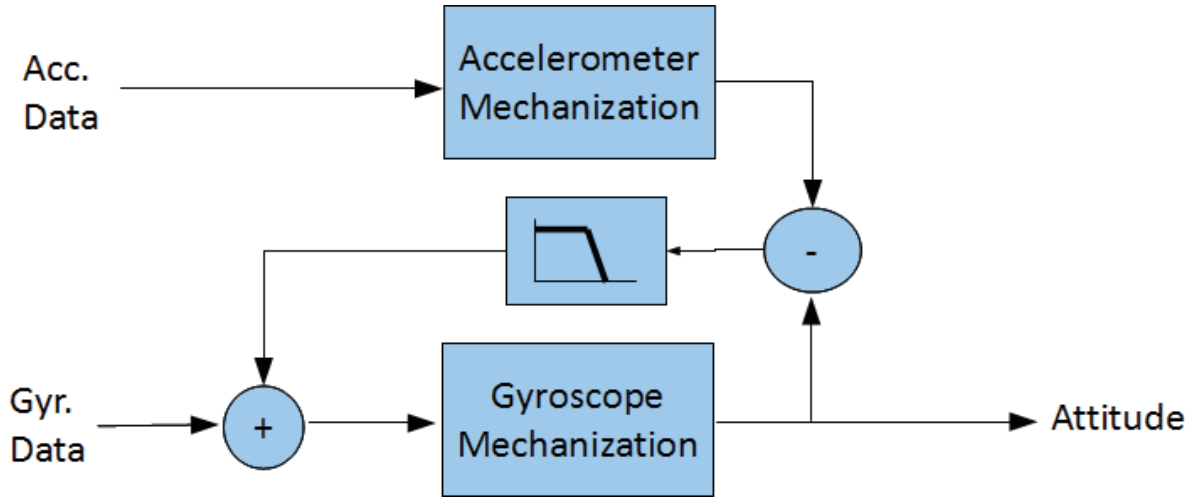

Figure 4.28 Attitude error feedback schematics; the feedback is provided to the gyroscope mechanization

To preserve the short-term dynamics processed correctly by the gyroscope mechanization from noise brought in by the accelerometer mechanization, filtering of the feedback was introduced. A simple low-pass filter was designed from using analog equivalent of a first-order system described by its transfer function:

$$T(s) = \frac{a}{s + a} \tag{4.2}$$

where ***s*** is complex Laplace operator and ***a*** is time constant of the system.

The algorithm takes rise time of the filter as the input parameter and then computes the time constant. Subsequently, discrete time equivalent was evaluated based on the signal sampling frequency. Thus, the algorithm is not dependent on the sampling frequency of the input signal. The feedback

signal is multiplied by a coefficient ***k*** and provided to the gyroscope signal integration. Simulation showed that the final closed-loop system may start oscillating, if the coefficient ***k*** is too high. Therefore, the feedback constants (**k** and ***rise time*** T_r) have to be chosen in such a way to ensure stable and efficient solution.

The proposed algorithm was tested on the Bellanca RC aircraft model measurements and on the real flight data, which are shown in Figure 4.29 and Figure 4.30. Comparison of the resulting RMS errors is shown in the Table 4.4.

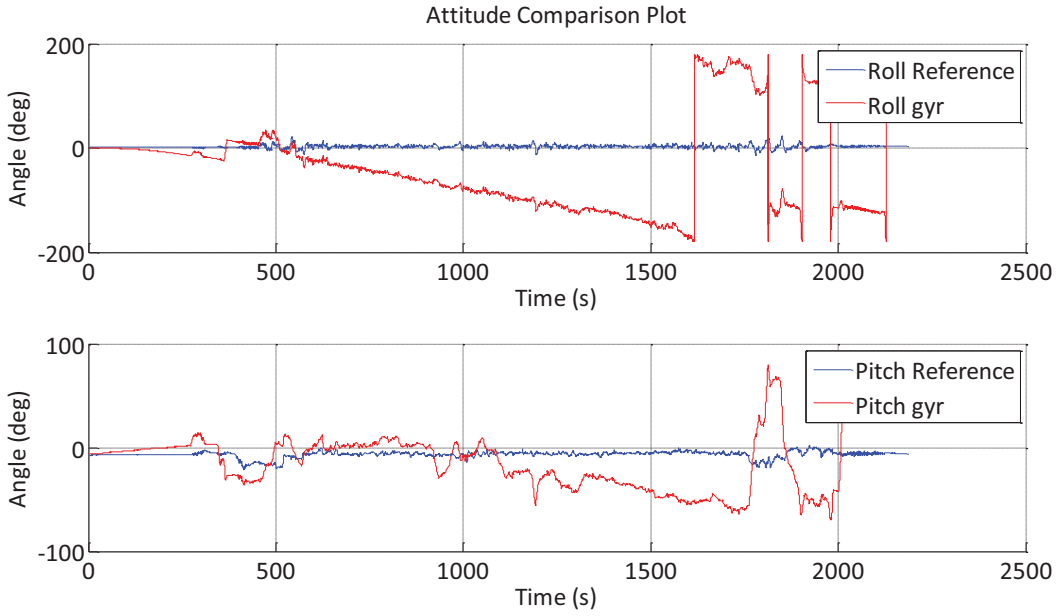

Figure 4.29 Roll and Pitch mechanization of the real flight data without the feedback

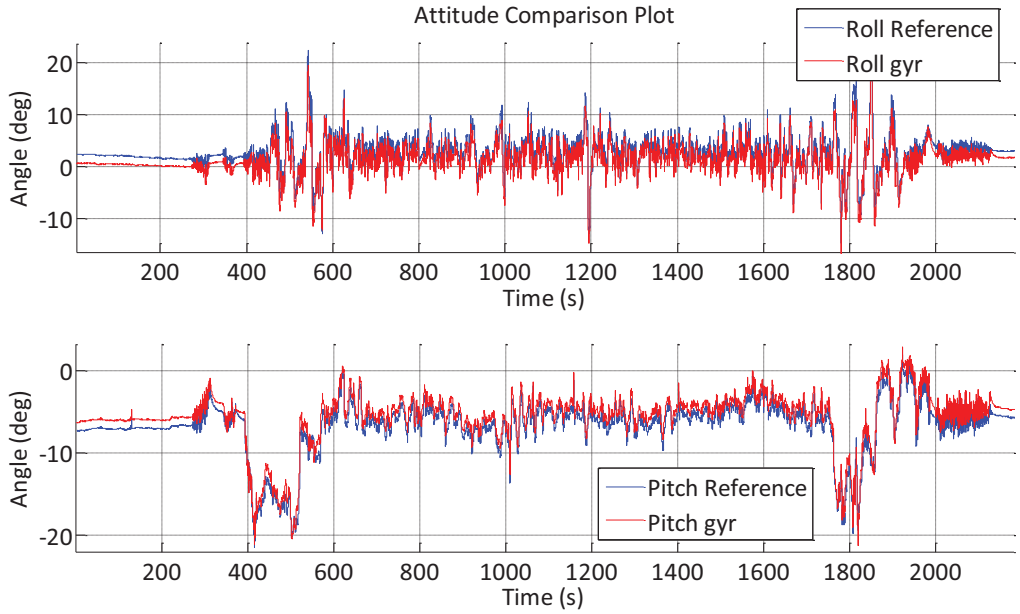

Figure 4.30 Roll and Pitch mechanization of the real flight data with the feedback and signal filtering

Feedback parameters: T_r = 20s K = 0.7	Length [s]	RMS error [°] : No feedback	RMS error [°]: Feedback and signal filtering	Improvement [°]
Bellanca shorter measurement	23.90	roll : 1.436	roll : 1.016	0.42
		pitch : 1.180	pitch : 0.327	0.85
Bellanca longer measurement	122.41	roll : 1.436	roll : 0.385	1.05
		pitch : 1.180	pitch : 0.288	0.89
Real flight data	2183.54	roll : 99.123	roll : 1.562	97.56
		pitch : 31.391	pitch : 1.034	30.36

Table 4.4 Improvements in accuracy of attitude mechanization with feedback and IIR/MA filters

The effect of the feedback was more evident in the case of a longer inertial measurement. It effectively prevented the gyroscope signal mechanization from drifting. The resulting attitude angles showed (in the case of a real flight data) a constant error of 1 degree. It is necessary to remind that the reference originated from the same inertial sensor, which performed its own mechanization. There are known issues with the onboard magnetometer, which was used as an aiding source for the mechanization. The main purpose of this demonstration was to confirm the ability to prevent the attitude drift and this was achieved.

The proposed correction feedback was unable to stop yaw angle from drifting because the coarse alignment could not determine the yaw angle. For this reason, the algorithm at the present form is not sufficient for the inertial navigation without any aiding signal sources, but still can be used in artificial horizon units. The position mechanization relies on the knowledge of the correct attitude including the yaw angle. After introducing additional signals, the feedback algorithm might be able to improve the accuracy of inertial navigation. Moreover, the output of the mechanization including the feedback showed a good dynamical behavior and a long-term stability.

The parameters of the feedback were determined experimentally with the aim to preserve the flight dynamics, suppress the gyroscope drift and the accelerometer coarse alignment introduced noise. As shown in the Table 4.4, the parameters were $T_r = 12s$ for the rise time of the filter and $k = 0.7$ for the feedback strength.

A similar algorithm was proposed by (Calusdian, Yun, & Bachmann, 2011).The proposed solution involves quaternion algebra based feedback and a magnetometer as an aiding source. A way of tuning a feedback coefficient was proposed in the paper taking in account angular velocity. This could be reconsidered for further investigation and a similar way of tuning coefficients mentioned in this work could be proposed.

5 Conclusion and Future Work

The goal of the work was to study an impact of vibrations and noise to inertial navigation accuracy and to design filters which would suppress this impact. Attitude mechanization was chosen to verify designed filters efficiency. These conclusions were made:

Allan Variance analysis

The noise terms of the ADIS16405 were determined using the AVAR method. Comparison with the datasheet showed an overall agreement; yet, the AVAR method discovered noise terms not mentioned in the datasheet; the presence of the quantization noise in the accelerometer signals was concerned reliable – the measurement error of the AVAR for the short-cluster averaging times is minor and the results were consistent. The other discovered noise terms were located in the long-cluster averaging times; therefore, the indicated values are less reliable. The results of the AVAR method may be used for the Kalman filter design, where the mathematical noise model accuracy is vital for its performance.

Vibration suppression

The spectral analysis, the filter design and the subsequent mechanization showed that mere filtering of the vibration does not significantly improve attitude mechanization performance. FIR, IIR, Wavelet and Moving Average filters were designed and tested. The compromise between preservation of body dynamics and vibration suppression was achieved using **IIR or FIR** filters with transition band from **16 to 24 Hz** for the gyroscope signal filtering and **Moving Average** filter of the **order of 100** (sampling frequency 320 Hz or the filter order scaled accordingly) for the accelerometer signal filtering. With these, the RMS error of **gyroscope attitude mechanization** was **diminished by 1.5°**; the RMS error of **accelerometer attitude mechanization** was **diminished by 2°**. The improvement concerns only RC plane measurement; no significant improvement was observed during RoTiP measurement mechanization. Different integration schemes were investigated. However, the difference between rectangular and trapezoidal integration scheme were found insignificant because of the high sampling frequency of 320Hz. The difference might be observed if a lower sampling frequency was chosen; nevertheless, it is not recommended in order to fulfill the sampling frequency criterion. Regarding future work, with a precise reference, the effect of vibrations on the position mechanization can be studied, while the effect of the vibrations on the attitude mechanization is known. However, a similar result is expected; the process of position mechanization involves double integration, which will show a drift disregarding the presence of harmonics caused by vibrations.

Drift suppression

The main source of error in gyroscope signal based attitude mechanization during long-term tests was the unbounded drift. An algorithm modification was proposed, introducing difference between accelerometer and gyroscope attitude mechanization as a feedback. The subsequent simulations confirmed its performance; the drift of the gyroscope signal mechanization was suppressed. The coefficients of the feedback were fine-tuned experimentally; the further work might aim to design an adaptive algorithm minimalizing the drift error. Overall RMS Error **under 1.6°** was achieved.

6 REFERENCES

Abdel-Hamid, W. (2005, January). Accuracy enhancement of integrated MEMS-IMU/GPS systems for land vehicular navigation applications. 82. DEPARTMENT OF GEOMATICS ENGINEERING, UNIVERSITY OF CALGARY .

Allan, D. W. (1966). Statistics of atomic frequency standards. *Proceedings of the IEEE, 54*(2), 221-230.

Altmann, J. (1996). *Wavelet basics*. Retrieved from Wavelet.org: www.wavelet.org/tutorial/wbasic.htm

Analog Devices. (2009). Triaxial Inertial Sensor with Magnetometer ADIS 16400/ADIS16405. *(B)*.

Burian, M. (2009). Zpracování signálů navigační jednotky. *Bachelor thesis*. Praha: CTU, Faculty of Electrical Engineering.

Calusdian, J., Yun, X., & Bachmann, E. (2011). Adaptive-Gain Complementary Filter of Inertial and Magnetic Data for Orientation Estimation. *2011 IEEE International Conference on Robotics and Automation* , (pp. 1916-1922). Shangai.

Crittenden, J., & Evans, P. (2008). MEMS Inertial Navigation System. *Student work*.

Curey, R., Ash, M., Thielma, L., & Barker, C. (2004). Proposed IEEE inertial systems terminology standart and other inertial sensor standarts. *Position Location and Navigation Symposium*, (pp. 83-90).

El-Sheimy, N., Hou, H., & Niu, X. (2008). Analysis and Modeling of Inertial Sensors Using Allan Variance. *Instrumentation and Measurement, IEEE Transactions on, 57*(1), 140-149.

Hopcroft, M. A. (2010). ALLAN. *MATLAB function, 2.22*.

IEEE. (1998). IEEE Standard Specification Format Guide and Test Procedure for Single-Axis Interferometric Fiber Optic Gyros. *IEEE Std 952-1997*, 62.

Keshner, M. (1982, March). 1/f Noise. *Proc. IEEE*, pp. 212-218.

Lawrence, C. N. (1993). On The Application of Allan Variance Method for Ring Laser Gyro Performance Characterization. USA: Lawrence Livermore National Laboratory.

MathWorks. (2008). Wavelet toolbox.

Meruane, C. C. (2008). Analysis and Modeling of MEMS based Inertial Sensors. *Thesis*. Royal Institute of Technology.

Reinštein, M. (2011). Use of adaptive filtering methods in inertial navigation systems. *Dissertation*. Praha: CTU.

Savage, P. G. (1998a). Strapdown Inertial Navigation Integration Part 1: Attitude Algorithms. *Journal of Guidance, Control, and Dynamics*(No. 1).

Savage, P. G. (1998b). Strapdown Inertial Navigation Integration Algorithm Design Part 2: Velocity and Position Algorithms. *Journal of Guidance, Control, and Dynamics*(No. 2).

Savage, P. G. (2005a). What Do Accelerometers Measure?

Savage, P. G. (2005b). What Do Inertial Sensors Measure?

Savage, P. G. (2006). What Do Gyros Measure?

Sazdovski, V., G., P. M., & Tsourdos, A. (2010). Inertial Navigation aided by Simultaneous Localization and Mapping. *Intelligent Systems (IS), 2010 5th IEEE International Conference*, (pp. 43-48).

Sedláček, M. (2009). Zpracování diskrétních signálů. In M. Sedláček, & V. Hlaváč, *Zpracování signálů a obrazů* (pp. 56-57). Praha: Czech Technical University.

SensorDynamics. (2011). *Mems structures*. Retrieved from SensorDynamics: http://www.sensordynamics.cc/cms/cms.php?pageId=51

Shin, E.-H. (2005). Estimation techniques for low-cost inertial navigation. Calgary, Canada: University of Calgary.

Skog, I., & Händel, P. (2006). Calibration of MEMS Inertial Measurement Unit. *XVII IMEKO WORLD CONGRESS.*

Sotak, M. (2010). Coarse alignment algorithm for ADIS16405. *Przeglad Elektrotechniczny, 86*(9), 247-251.

Strang, G., & Nguyen, T. (1997). *Wavelets and Filter Banks.* Cambridge: Wellesley-Cambridge Press.

Šipoš, M. (2010). TRIAXIAL ACCELEROMETER CALIBRATION. *MATLAB software*.

Welch, P. (1967). The Use of Fast Fourier Transform for the Estimation of Power Spectra: A Method Based on Time Averaging Over Short, Modified Periodograms. *IEEE Transactions on Audio Electroacoustics*(Volume AU-15).

Žoha, J., & Fejfar, O. (2008). Řídicí systém pro testovací platformu.

7 ANNEX A: ALLAN VARIANCE PLOTS

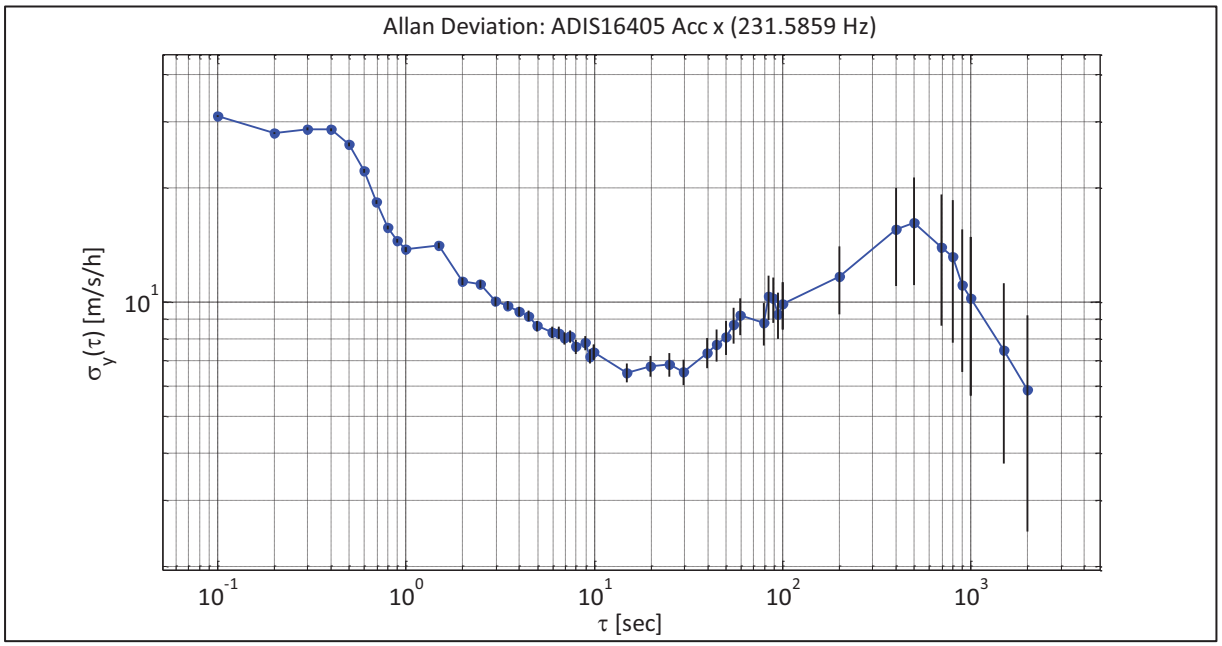

Figure A.1 Root AVAR of the accelerometer signal x

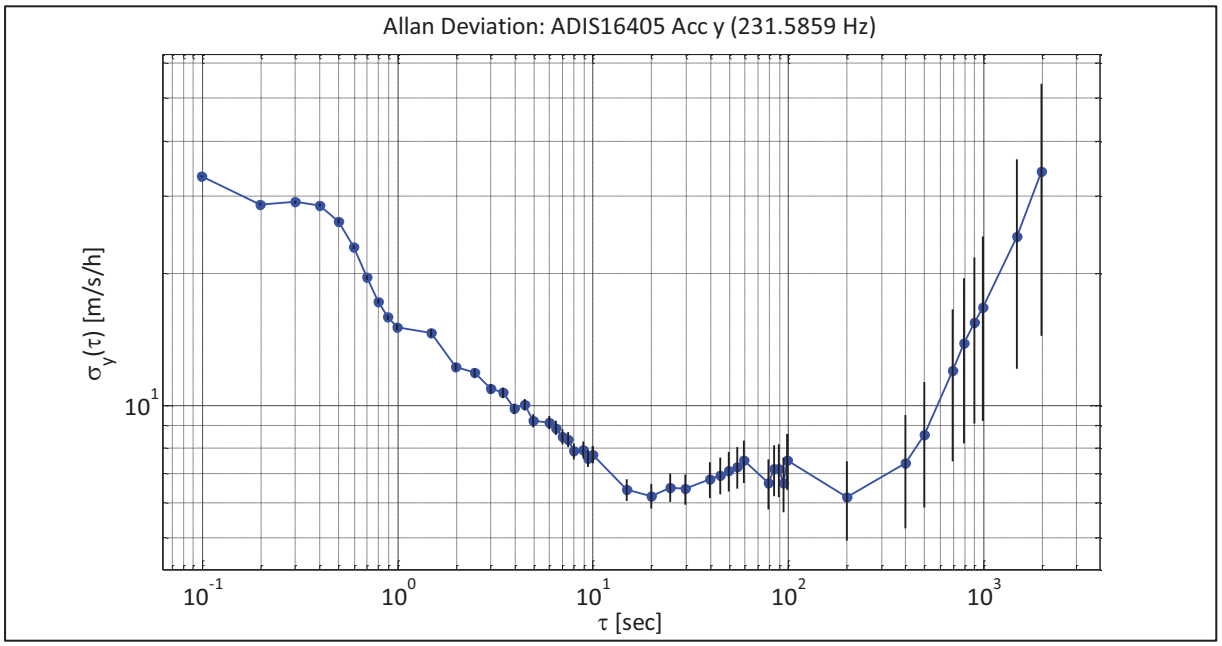

Figure A.2 Root AVAR of the accelerometer signal y

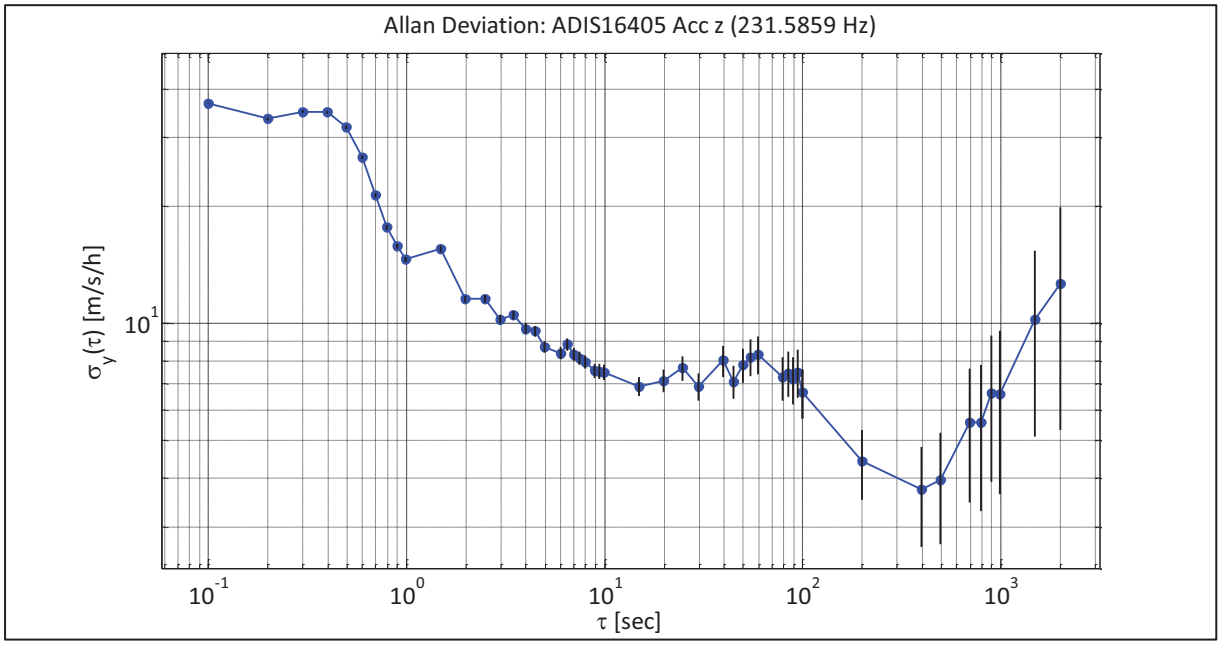

Figure A.3 Root AVAR of the accelerometer signal z

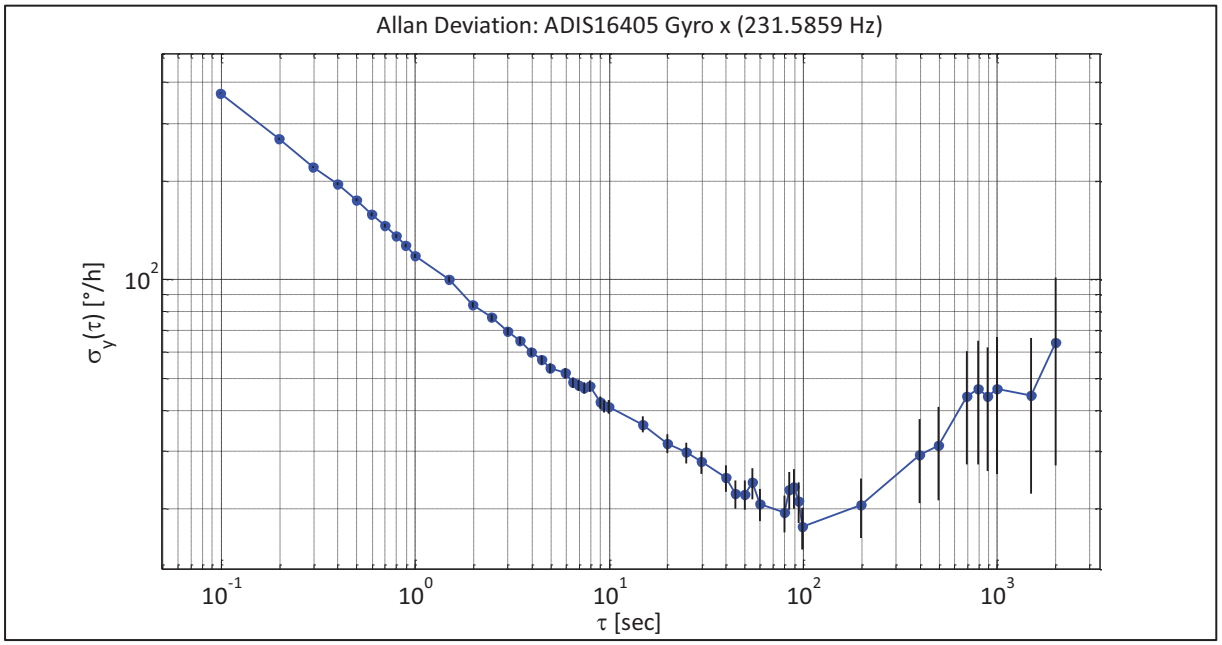

Figure A.4 Root AVAR of the gyroscope signal x

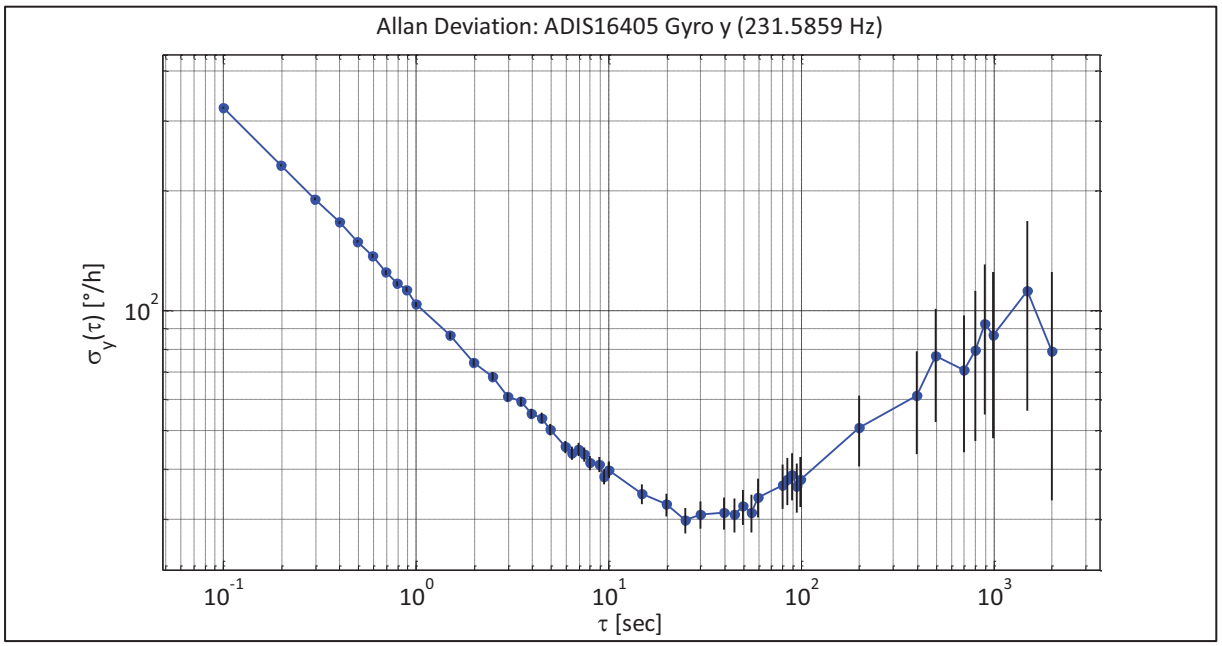

Figure A.5 Root AVAR of the gyroscope signal y

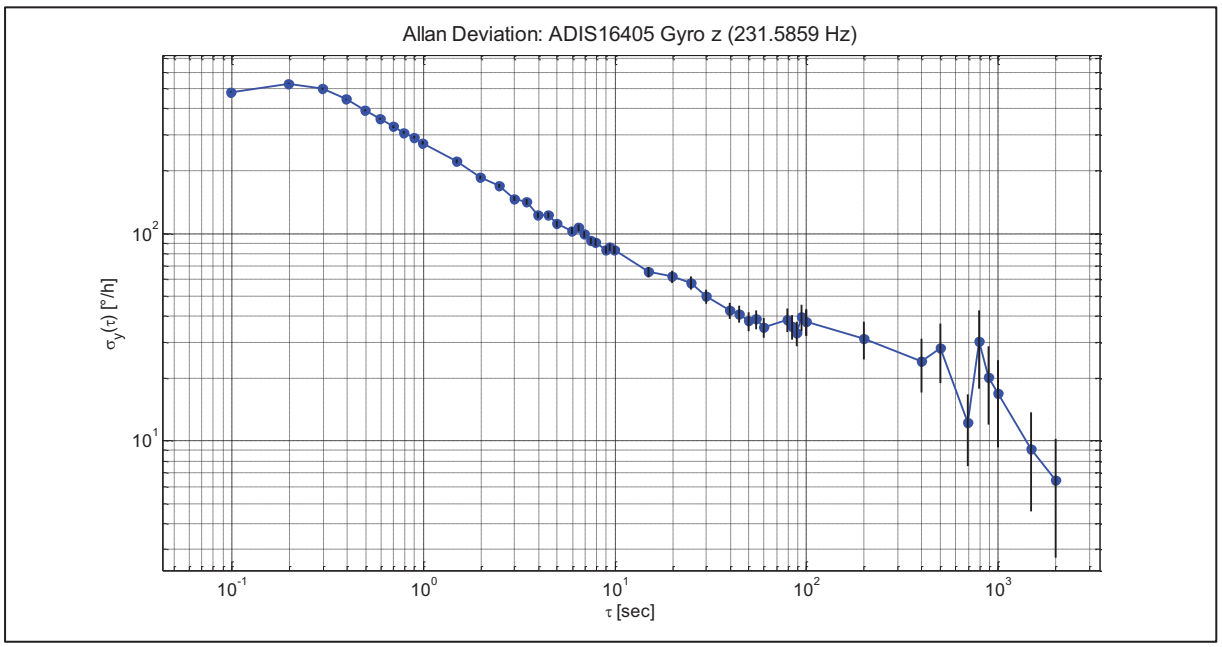

Figure A.6 Root AVAR of the gyroscope signal z

8 ANNEX B: CALIBRATION TABLE ROTIP

The calibration table RoTiP (Figure B.1) was used in several experiments. It provided precise attitude control and reference output. The table platform rotates in sense of roll, pitch and yaw; therefore, the application of the RoTiP was straightforward and there was no need of reference data processing. The platform could be controlled using a graphic user interface installed on a PC and connected via RS232.

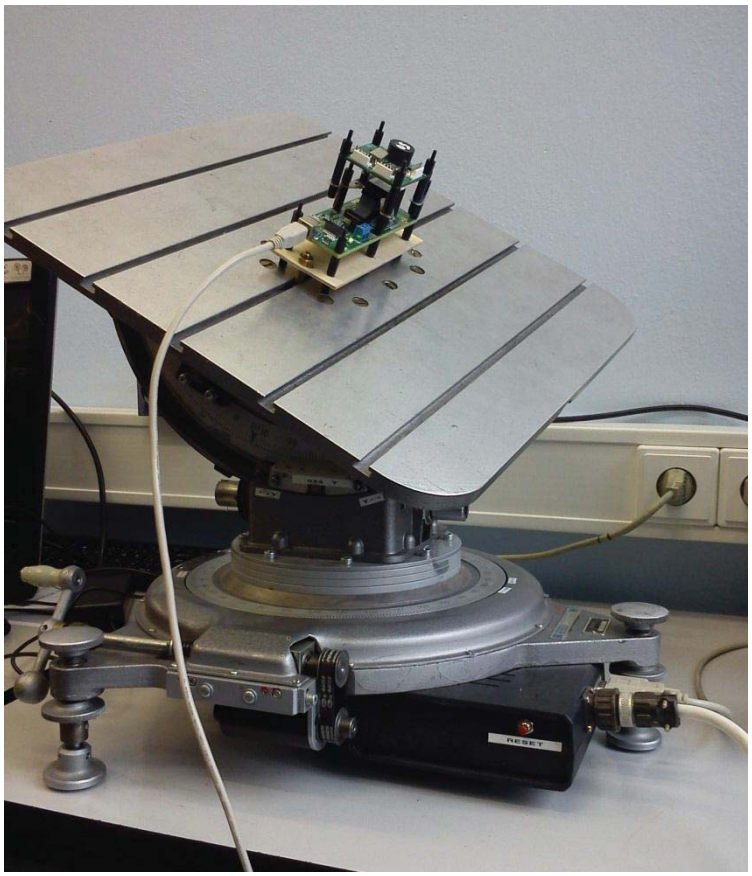

Figure B.1 Calibration table RoTiP with the ADIS16405 attached

The platform was calibrated each time using a precise inclination meter Clinotronic PLUS CH-8405. Once calibrated, these parameters were provided (Žoha & Fejfar, 2008):

Roll angle: ± 45° with resolution 1.15''

Pitch angle: ± 30° with resolution 2.3''

Yaw angle: unbounded with resolution 2.6''